Controlling Long-Range Ordered Self-assembly of Solid-Binding Peptide Monolayers on Atomically Flat Layered Materials

David Alan Starkebaum

A thesis

submitted in partial fulfillment of the

requirements for the degree of

Masters of Materials Science and Engineering

University of Washington

2016

Committee:

Mehmet Sarikaya

Bruce Hinds

Xiaodong Xu

Program Authorized to Offer Degree:

Materials Science and Engineering

University of Washington

Abstract

Controlling Long-Range Ordered Self-assembly of Solid-Binding Peptide Monolayers on Atomically Flat Layered Materials

David Alan Starkebaum

Chair of Supervisory Committee:

Professor Mehmet Sarikaya

Materials Science and Engineering,

Chemical Engineering, and Oral Health Sciences

Solid-binding short peptides offer great promise as molecular building blocks in nanotechnology and nanomedicine. Some of these peptides can form self-organized nanostructures on solid surfaces due to highly specific coordination of inter-molecular forces enabled by conformational changes in the peptide. This study aims to examine how the organization of self-assembled monolayers formed by a phage display selected "wild-type" graphite binding peptide (GrBP5-WT) change with solution conditions, such as pH and ionic strength. The surface coverage and crystallinity of these peptide monolayers were shown to increase when incubated in 1mM sodium phosphate. In contrast, GrBP5-WT incubated in 1mM sodium hydroxide showed significantly decreased coverage, and no long-range-ordered structures. Zeta potential measurements of aqueous graphite powder dispersions showed a pH-dependent negative surface

charge, which increased in magnitude when GrBP5-WT was added. A peptide mutant (GrBP5-M9) was designed by replacing two carboxylate residues with polar, but non-charged, amide residues. The mutant peptide formed crystalline nanostructures on graphite, which were unaffected by changes to the ionic strength or pH, and did not contribute additional negative charge to the graphite dispersion zeta potential. This showed that a simple mutation to a phage-display selected solid-binding peptide can eliminate its sensitivity to buffer and pH changes, facilitating the formation of more predictable bio/nano interfaces towards the development more robust biosensors and bioreactors.

Self-assembly of GrBP5-WT and two other mutants (M6 and M8) was also shown on a variety of different atomically-flat 2D solid substrates, including CVD graphene on copper, and exfoliated BN, MoS_2, $MoSe_2$, WS_2, and WSe_2 on SiO_2/Si. Although long-range ordered structures were shown on each substrate material, subtle differences in the patterns formed on each substrate indicate an important influence of the underlying crystal structure on the peptide nanostructure. The ready formation of ordered nanostructures opens the door for an investigation of the physical properties of number of hybrid nanomaterials. In particular, solid-binding peptides were shown to induce a molecular doping effect on the photoluminescence of single-layer $MoSe_2$ (a 2D semiconductor with a direct band-gap in the visible light spectrum). Peptide self-assembly was also found to be sensitive to the presence of polymer residues commonly used in lithographic processing (such as PMMA). Indium microsoldering was investigated as a means to prepare electronic devices (such as graphene field-effect transistors) without contaminating the substrate.

TABLE OF CONTENTS

FIGURE CAPTIONS

ACKNOWLEDGEMENTS

I would like to thank Professor Mehmet Sarikaya for accepting me into the graduate program at the University of Washington, and for his ongoing support throughout the years. I am also grateful for all of the advice, contributions, and support from colleagues in the Sarikaya group. Specifically, I would like to thank Professor Yuhei Hayamizu for helping me to get started with the buffer/pH study and many other projects, Dr. Hanson Fong for a variety of advice and support, Dr. Chris So for his patient advice regarding peptide self-assembly and atomic force microscopy procedures, Dr. Dmitriy Khatayevich for advice about graphene FET biosensor design, Tamon Page for his tireless effort as we worked together on the pH/buffer study, Carolyn Gresswell for helping with peptide synthesis, Deniz Yucesoy for coming up with the idea for the glucose oxydase biosensor project, and Wentao Lu for his help with indium micro-soldered graphene field effect experiments. I would also like to thank the many collaborators from other research groups, including Professor John Berg and his (former) student Dr. Matthew Gacek for help with the Zeta potential measurements; Professor Xiaodong Xu, and his students Jason Ross and Genevieve Clark for their help with the $MoSe_2$ and WSe_2 photoluminescence experiments; Professor Valerie Daggett and her (former) student Dr. Chin Jung Cheng for their help with the molecular dynamics simulations; and Dr. Jeremy Robinson for his help with the CVD graphene experiments. I would also like to thank the many undergraduates who have helped me with a variety of experiments, including Jordan Holmes, Michale Dymond-Shaw, Jackson Bloom, and Davis Tran. I would like to thank Eve Riskin, Sonya Cunningham, Scott Winter, Dave Prince, Lynne Spencer in the College of Engineering STARS program for supporting me as a teaching assistant while I carried out this research. I would also like to thank my parents, Mary and Gordon Starkebaum, for their steadfast support (financial, moral, and academic) throughout this process. I am also grateful to my wife, Mari, and two children, Maia and Soeskay, for their patience through many long hours and late nights.

This research was supported by NSF-Biomaterials (DMR-0706655) and MRSEC program (DMR-0520567) at GEMSEC, Genetically Engineered Materials Science and Engineering Center, University of Washington. YH was supported by JST PRESTO program (Japan) and also by NSF MRSEC program. TRP, DAS, and MS were supported by MRSEC. JH was an REU in this project. The work was carried out at the GEMSEC-SECF, a member of Materials Facilities Network of MRSEC.

INTRODUCTION

Solid-binding peptides have been developed by combinatorial mutagenesis to recognize and bind with high affinity to specific inorganic solids, such as gold, platinum, titanium oxide, or hydroxyapatite. [2-5] These peptides can further be formed into multi-functional constructs, providing a unique means to bridge solid inorganic materials with biological systems at the molecular scale. This has a number of potentially useful applications, including enzyme immobilization, [1] bio-functionalization of implants, [2, 3] and signal transduction in biosensors. [4] Furthermore, since peptide monolayer coatings are prepared at ambient temperature from aqueous solutions, they are better suited to biological conditions than other self-assembling monolayer systems, such as silanes, thiols, and phosphonates, which require organic solvents. [5-7] Although they have relatively short sequences (7~14 amino acids), these peptides bind strongly (dissociation constant, K_d = 50nM~1μM) through non-covalent intermolecular forces *via* the combined effect of multiple contact points. [9, 10]

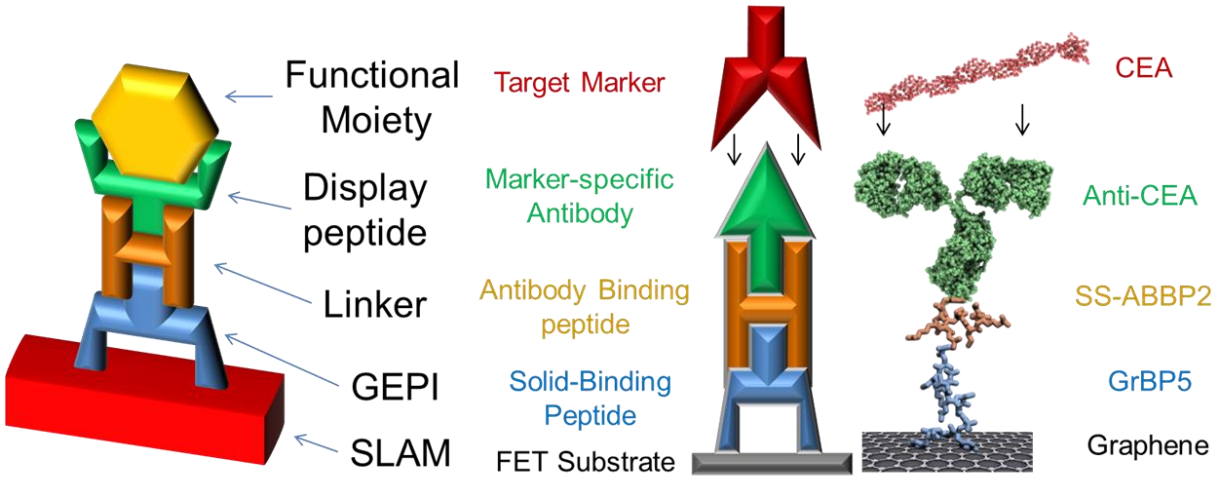

Figure 1: Schematic of a modular peptide linker for controlled immobilization of target molecules on a solid surface. Khatayevich *et al*, "Multifunctional Peptide Enabled Graphene Nano-Sensor Platform for Cancer Marker Screening", *To be submitted* 2013

In addition, certain solid-binding peptides have also been found to spontaneously self-assemble into long-range-ordered mono-molecular thin films on atomically flat surfaces. [8] Identifying optimum conditions for such self-assembly would be highly valuable, especially in light of potential biological and medical applications. This study aims to examine the effects of varying solutions conditions (pH, buffer), and peptide mutations on self-assembled peptide nanostructures formed on graphite. Further studies examine the self-assembly on different substrates besides graphite, and characterize the effect of peptides on the optoelectronic properties of 2D semiconductor materials.

SUBSTRATE MATERIALS: GRAPHITE AND GRAPHENE

Direct experimental observation of the interaction of engineered peptides with solids requires a surface with well-defined atomic-scale topography, crystal structure, and surface chemistry. It is also imperative that these properties are persistent under biological conditions (aqueous electrolyte), not just under high vacuum and in a clean room. These requirements have recently been realized with 2D solids, such as layered dichalcogenides, nitrides, and carbides, and graphite. [9-11] Mechanically-exfoliated highly-oriented pyrolitic graphite (HOPG) satisfies all of these conditions, providing large, clean, flat surfaces ideally suited for atomic force microscopy (AFM).

Graphite has an anisotropic crystal structure consisting of sheets of carbon atoms which are held together by Van der Waals forces (lattice constants: a = 2.46Å, c = 3.35Å)[12]. In the solid crystalline form, these carbon layers typically stack in an ABAB arrangement, giving the overall crystal structure a $P6_3mmc$ space group. However, stacking faults are common, either in the form of ABC stacked layers, or rotational faults (where individual or groups of layers are rotated relative to the layers above and below).

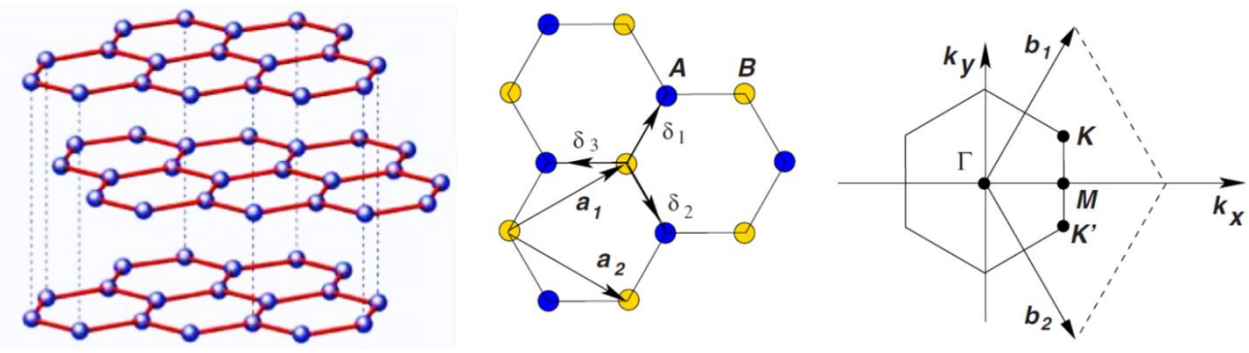

Figure 2: Graphite crystal structure, atomic lattice, and Brillouin zone. Neto *et al*, "The electronic properties of graphene", *Rev. of Modern Physics*, 2008 [13]

Graphite has excellent electrical conductivity, due to the long-range delocalization of the sp2-hybridized (π-bonded) electron orbitals that stretch across the entire basal plane. This is similar to conductive polymers such as polyaniline, which conduct electrons through conjugated (π-bonded) electrons. This high electrical conductivity leads to high thermal conductivity also, as thermal energy can be carried by the fast-moving electrons, in addition to phonons in the atomic lattice.

Graphite has established applications as an electrode material, [14] a solid-state lubricant, [15] and as a structural material in heart valve implants. [16] Furthermore, graphite can act as an analog for graphene, which has a wide range of potential applications due to its anti-microbial activity, [11] efficient thermal conductivity, optical transparency, [17] and surface-sensitive electrical conductivity. [12-14]

In 2004, Novoselov and Geim demonstrated the "scotch tape method" for mechanical exfoliation of graphene (single atomic layer graphite) on Si/SiO_2, and measured the electronic properties of graphene field-effect transistors. [17] Graphene electronic properties are typically characterized in the "field-effect transistor" (FET) configuration, consisting of "source", "drain", and "gate" electrodes on an insulating surface such as SiO_2. The Fermi energy of the graphene sheet can thus be controlled by applying a voltage between the graphene and the P-doped silicon

wafer "gate". If the "source-drain" voltage across the graphene channel is held constant, the current passing through the graphene channel tends to increase linearly with the gate voltage. This increase in conductivity is attributed to an increase in the concentration of free charge carriers in the channel. Unique to graphene, an increase in conductivity occurs for both negative and positive gate voltage, giving a property known as "ambipolar conductivity". That is, the graphene can support a current of either electrons (with a negative charge) or "holes" (with a positive charge).

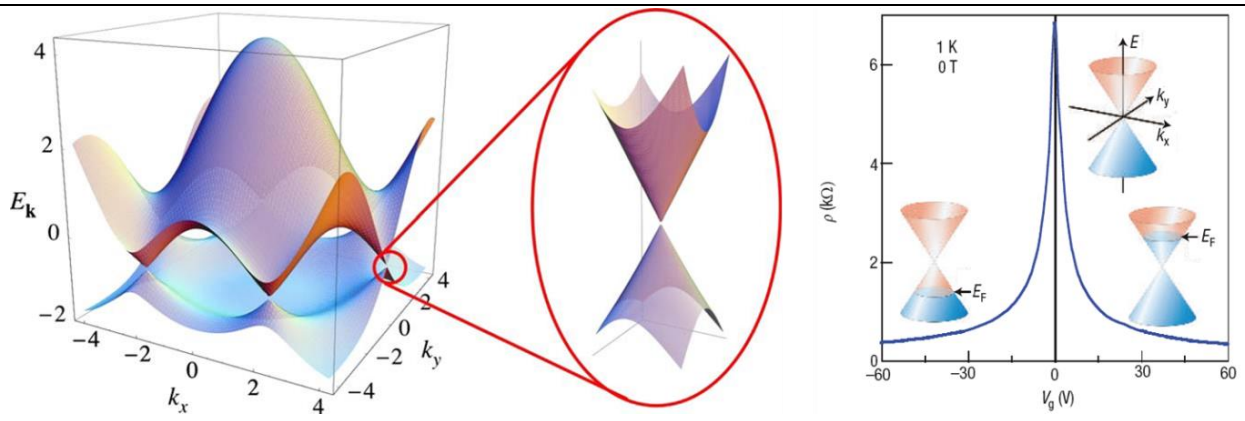

Figure 3: Graphene band structure, showing the "Dirac Point" where the valence band meets the conduction band. Neto *et al*, "The electronic properties of graphene", *Rev. of Modern Physics*, 2008 [13]

The valence band (bonding orbitals) and the conduction band (antibonding orbitals) of graphene meet at the "K-point" in the Brillouin Zone, corresponding to the periodic wave function along the $[11\bar{2}0]$ family of unit vectors in the atomic lattice. This gives graphene the unique characteristic of a "zero-gap" semiconductor, or "semi-metal". Thus, if the graphene is highly pristine (with no molecular contamination), there will be a minimum in the conductivity when no gate voltage is applied. This is known as the "charge neutral point" (CNP), and occurs when the Fermi-energy is set at the cross-over point between the valence and conduction bands. [13]

If another material is brought into contact with graphene, there will be a certain amount of charge-transfer into or out of the graphene sheet (depending on the relative Fermi energy of the other material). When this effect occurs due to adsorbed molecules, it is known as "charge-transfer doping". This phenomenon is similar to the impregnation of semiconductors (such as silicon) with group III or V "doping" impurities to increase their conductivity.

Another possible doping mechanism involves the formation of "image charges" in graphene in response to the proximity of charges adsorbed to the surface. In this case, a positively charged molecule would attract a negatively charged electron to the graphene surface (from the "ground", or pool of available electrons in an attached metal electrode). This would result in charge carriers in the graphene of opposite charge to the absorbed molecules. This mechanism can also occur with the absorption of molecules with a large dipole moment, even when the net charge is zero.

It should be noted that: Most real graphene FET devices supported by a 300nm SiO_2 dielectric require +20V to be applied to the gate graphene to reach the CNP. This is usually due to the presence of various contaminations from the air (such as absorbed volatile organic compounds), and/or from trapped charge impurities in the SiO_2 dielectric. [18]

In the case of bulk graphite, any changes to the charge-carrier density (and thus, conductivity) due to molecular absorption on the top layer will have a minimal effect on the overall conductivity, since there are a near-infinite number of alternative routes for electrons to travel through deeper layers. Thus, single-layer graphene has a distinct sensitivity to these "surface effects" not found in bulk graphite.

These unique electronic properties make graphene an ideal material for biosensor applications[19]. The idea here is that one can detect the absorption of molecules to the graphene surface by monitoring the current through the graphene channel as the surface is exposed to

different environments. The graphene channel will respond dramatically to any changes in the environment, due to the "molecular doping" effect. The challenge is to isolate one particular signal from all of the noise. This is where peptides can serve a unique function. [4]

Characteristics of Peptide Self-Assembly

Peptide self-assembly allows for (i) control of arrangement and orientation of molecular dipoles on the solid surface, and (ii) the specific immobilization of specific target molecules (such as hormone or antigens). Control of molecular dipoles on the surface leads to more predictable effects on the substrate. When molecules are absorbed randomly on the graphene surface, the measured effect is an "averaging" of the contributions of these many different orientations. This often leads to weaker overall doping, as oppositely-aligned dipoles can partially cancel out each other's contributions. Furthermore, each absorbed molecule can cause irregular changes to the local electric field, resulting in point-defect scattering of conducting electrons. [20] The result is a drop in overall electron mobility, and a loss in efficiency in the circuit (increasing dissipative losses, and requiring higher voltages to operate).

When the absorbed peptides are regularly arranged in long-range ordered structures, two effects emerge. First, the molecular doping effect is amplified, as the dipoles from individual molecules are aligned in the same direction (leading to a "super-molecular dipole"). Furthermore, the charge-mobility in the graphene channel is increased, since the ordered peptides form a (nearly) commensurate lattice with the graphene crystal, and point-defect scattering is minimized.

Ordered peptides on the graphene surface offer an additional unique advantage: controlled orientation of the molecule allows for control of the surface chemistry. Based on knowledge of

the peptide morphology and orientation on the graphene surface, mutations can be made to the peptide sequence which specifically modifies the domain exposed to the solution.

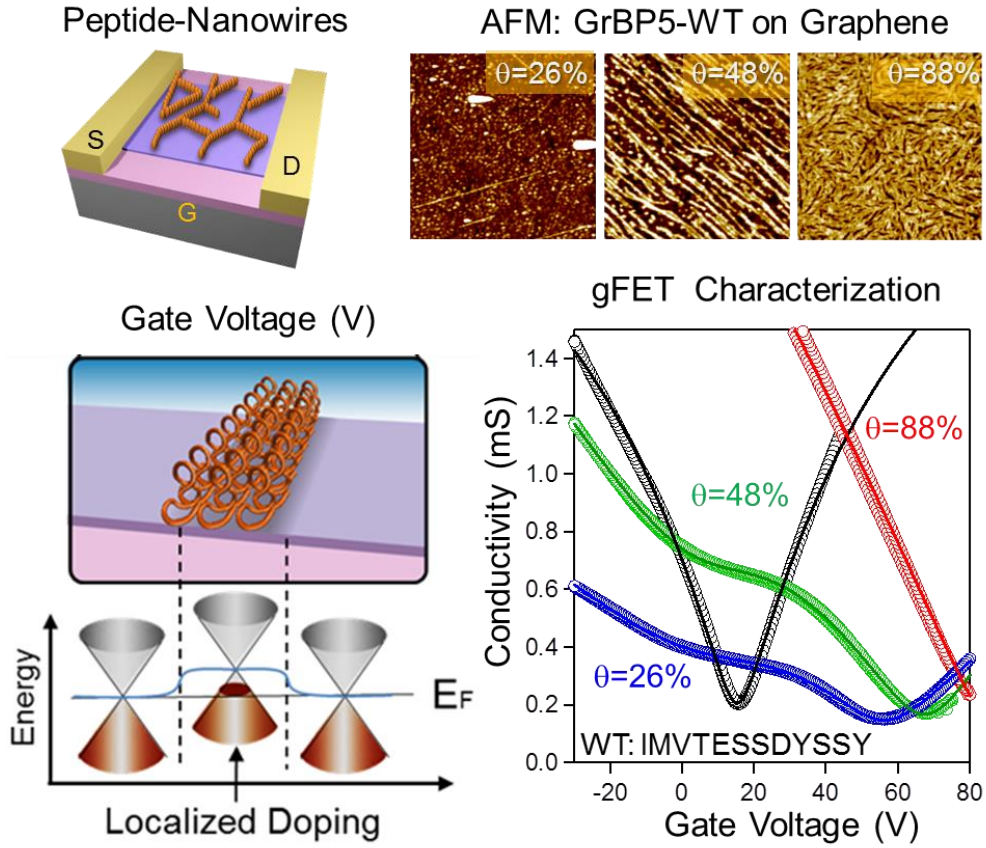

Figure 4: Effect of peptide nanowires on the electronic properties of graphene field effect transistors. From: Hamaizu *et al*, "Bioelectronic interfaces by spontaneously organized peptides on 2D atomic single layer materials", *Scientific Reports,* under review

Previous studies have demonstrated mutations which can control surface energy (water droplet contact angle). This can lead to the formation of an "anti-fouling" layer which tends to discourage the non-specific absorption of undesired proteins from the surface. Alternatively, specific amino acid sequences (or other bio-active moieties), which allow for the immobilization of specific targets (such as streptavidin), can be spliced onto the peptide. A combination of these two behaviors can allow for highly specific and sensitive detection of target molecules in a mixed solution.

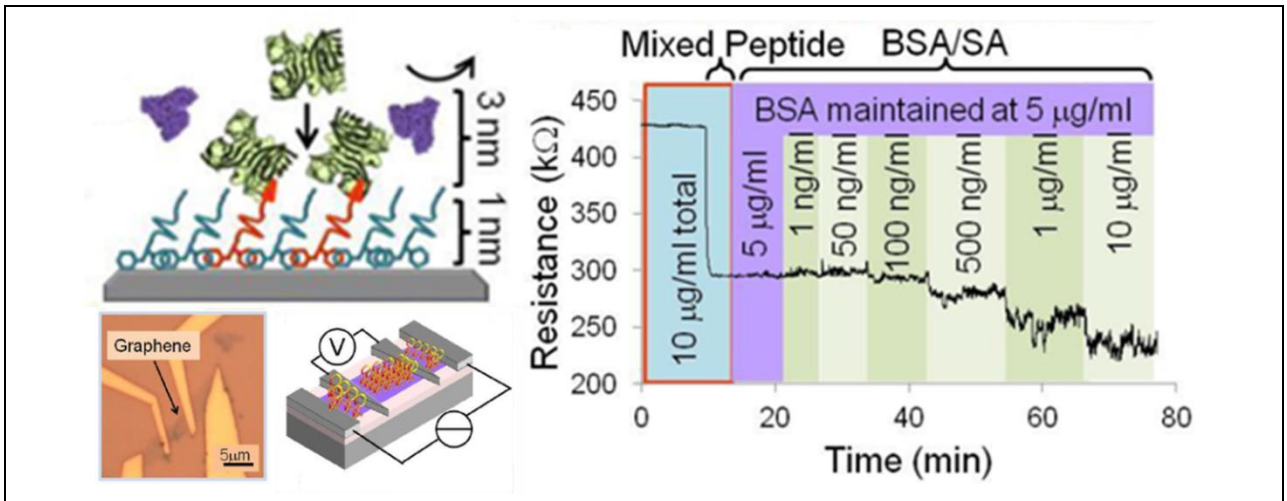

Figure 5: Device architecture for detection of a specific analyte in a mixed solution using a peptide-enabled graphene field-effect transistor biosensor, from: Khatayevich *et al*, "Selective Detection of Target Proteins by Peptide-Enabled Graphene Biosensor", *Small*, 2014

Previous Studies of Graphite-Binding Peptides

Previous studies have provided a number of clues to the necessary conditions to achieve self-assembly of peptides onto graphite in a molecular monolayer with long-range ordered structures, and the processes by which this occurs. The 12-mer "Wild-Type" graphite-binding peptide used in my studies, GrBP5-WT (amino acid sequence IMVTESSDYSSY), was selected from a phage display library based on affinity to solid graphite powder. [21] This peptide was found to spontaneously self-assemble into a mono-molecular thin-film on HOPG.

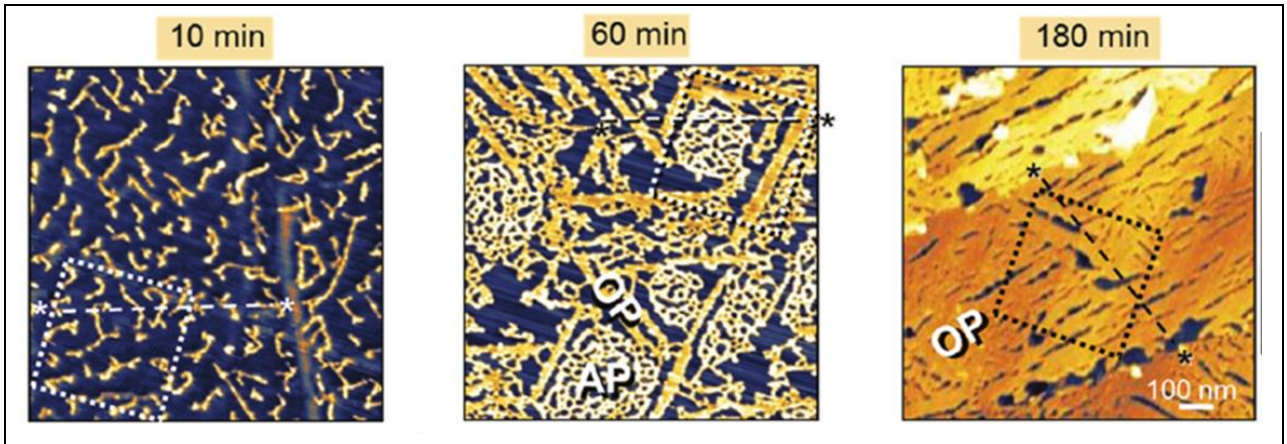

Figure 6: Effect of incubation time on peptide self-assembled structure. So *et al*, "Controlling Self-Assembly of Engineered Peptides on Graphite by Rational Mutation", *ACS Nano*, 2012

The surface coverage and ordered structure was found to depend significantly on the peptide concentration, as well as on incubation time. A peptide concentration of 1µM incubated at room temperature on graphite for 1 hour produced a mix of aligned "peptide nanowires" interspersed with amorphous regions. Increasing the peptide concentration to 1µM, or the incubation time to 3 hours, resulted in a densely-packed confluent monolayer film, largely aligned into ordered structures. Decreasing the peptide concentration below 500nM, or the incubation time down to 10 minutes, resulted in the formation of sparse peptide clusters or islands, with few ordered nanowires.

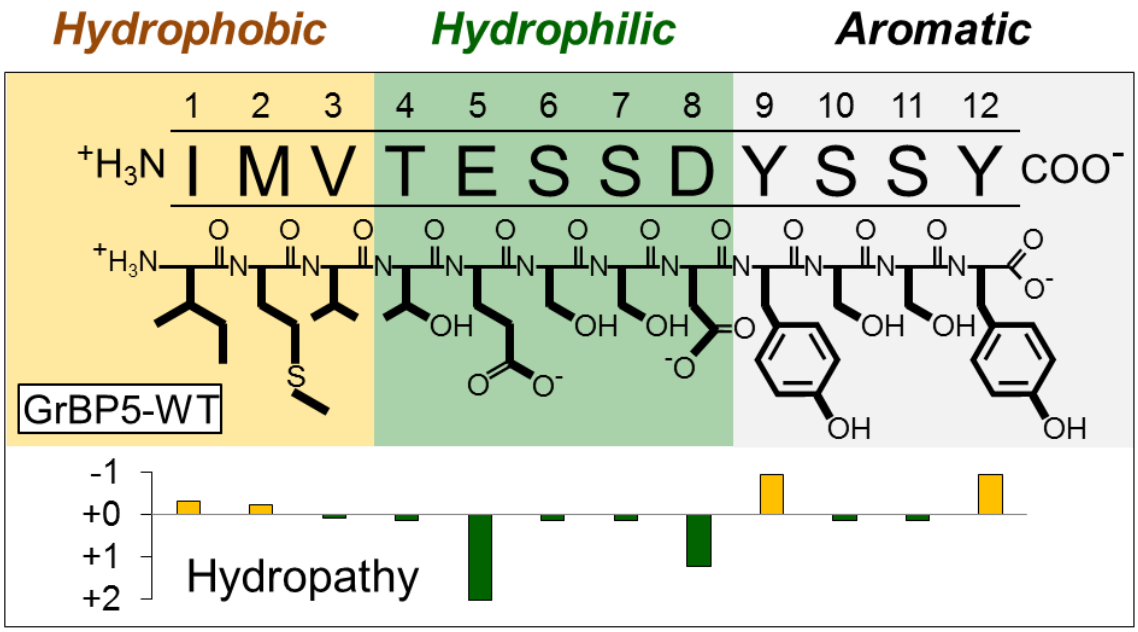

Figure 7: Properties of GrBP5-WT peptide. The amino acid sequence is broken down into three functional domains based on the nature of the amino acid side-chains: hydrophobic, hydrophilic, and aromatic. The "average free energy change of absorption to a phospholipid bilayer interface" (Wimley, White, *et al*) [30] of each amino acid side chain is shown below the peptide sequence. Units are given in kcal/mol. Values above the horizontal axis (shown in gold) indicate hydrophobic residues, while values below the horizontal axis (shown in green) indicate hydrophilic residues. Starkebaum *et al*, "Controlling the Self-Organization of Graphite-Binding Dodecapeptides in Varying pH and Ionic Strength" Acta Biomaterialia, *To be submitted*.

Mutations to the peptide sequence can allow for detailed probing of the role of each amino acid in the self-assembly process. By this method, it was established that the aromatic tyrosine

residues in the "head" domain (YSSY) are primarily responsible for the initial binding to the graphite surface. Replacing these with alanine (ASSA) leads to a dramatic loss of surface coverage for the same peptide concentration. Replacement of the tyrosine residues with larger aromatic tryptophan residues (WSSW) tended to increase the peptide coverage, but resulted in entirely amorphous peptide films.

Replacement of the hydrophobic "tail" domain (IMV) with hydrophilic residues (TQS) led to minimal changes in overall peptide coverage, but resulted in a loss of long-range ordered structures. However, a different hydrophobic peptide sequence in the "tail" domain (LIA) actually maintained the long-range ordered structures found in the WT peptide.

The conclusion is that a careful balance of hydrophobic (IMV), hydrophilic (TESSD) and aromatic (YSSY) domains are necessary for the formation of long-range ordered peptide nanostructured on graphite. Furthermore, the process of peptide self-assembly on graphite in aqueous solution can be attributed to a combination of surface diffusion, and changes to the peptides orientation and conformation.

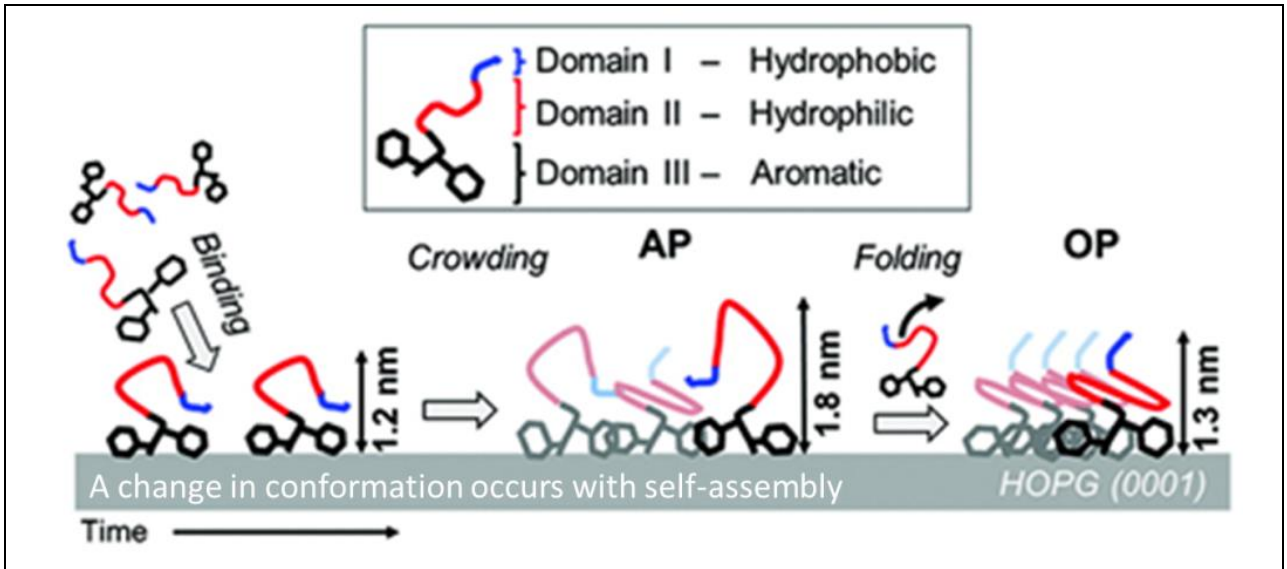

Figure 8: Model of peptide self-assembly, broken down into stages of binding, diffusion, and conformational change. So *et al*, "Controlling Self-Assembly of Engineered Peptides on Graphite by Rational Mutation", *ACS Nano*, 2012

EFFECTS OF PH AND BUFFER ON PEPTIDE SELF-ASSEMBLY

In this study, we examined the effects of phosphoric acid, sodium phosphate and sodium hydroxide on the binding affinity and self-assembled morphology of two graphite-binding peptide mutants on HOPG. The first mutant is GrBP5-WT, the same peptide used in previous studies. The second peptide, GrBP5-M9 (IMVTQSSNYSSY), is a mutant of the WT peptide in which two carboxylic acid residues (4-glutamic acid and 7-aspartic acid), were replaced with two amide residues (4-glutamine and 7-asparagine). Although the two acidic side-chains were removed, the "net charge neutral" peptide (M9) still carries zwitterionic charges at the N- and C-termini, which can each change their protonation state under extreme pH conditions.

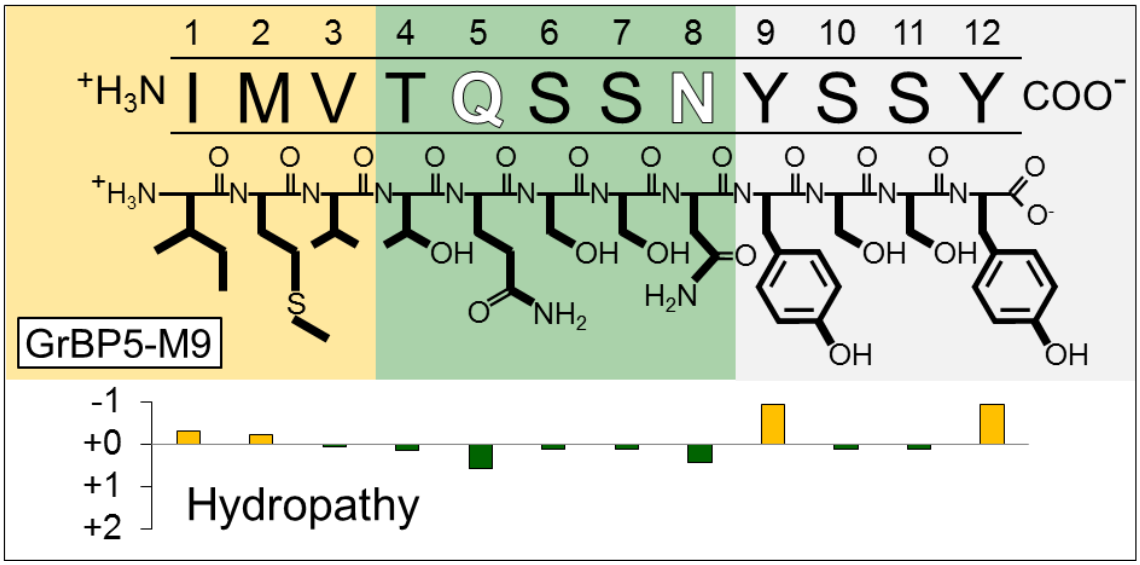

Figure 9: Properties of GrBP5-M9 peptide, in which glutamic acid (E) and aspartic acid (D) of the WT peptide were replaced with asparagine (Q), glutamine (N). As with the WT peptide sequence, the "average free energy change of absorption to a phospholipid bilayer interface" (Wimley, White, *et al*) [30] of each amino acid side chain is shown below the peptide sequence.

MATERIALS AND METHODS

PEPTIDE SYNTHESIS

Peptides were prepared on an automated solid-phase peptide synthesizer (CS336X, CSBio Inc., Menlo Park, CA) employing standard batchwise *Fmoc* chemistry procedures as reported

previously.[21] The crude peptides were purified by reverse phase high performance liquid chromatography to >98% purity (Gemini 10μm C18 110A column) and verified by MALDI-TOF mass spectrometry (Bruker Daltonics Inc., USA). The monomeric state of peptides in solution was also verified *via* size-exclusion chromatography. Peptides were lyophilized after synthesis and stored in a -80°C freezer for later use. Dilute stock solutions (20~100μM) were prepared by dissolution and dilution of lyophilized peptide in de-ionized water (16.1MΩ/cm).

PREPARATION OF PEPTIDE SOLUTIONS WITH ELECTROLYTES.

10mM phosphoric acid (H_3PO_4) stock was diluted from 85% (14.74M) phosphoric acid from Avantar Performance Materials Inc. (Center Valley, PA). 10mM stock solutions of sodium phosphate and sodium hydroxide were prepared from solid disodium phosphate, heptahydrate (Na_2HPO_4-$7H_20$, 268.07 g/mol) from Mallinckrodt Baker Inc. (Phillipsburg, NJ), and solid sodium hydroxide (NaOH, 98%) from Sigma Aldrich (St. Louis, MO) dissolved in de-ionized water.

Peptide and buffer stock solutions were combined to prepare a series of 1μM peptide solutions in 10μM~1mM NaH_2PO_4, as well as in 1mM H_3PO_4 and 1mM NaOH. The pH and temperature of each prepared solution was measured by an UB-10 UltraBasic pH/mV meter from Denver Instruments (Denver, CO), calibrated using pH 4.00, 7.00, and 10.00 pH buffer solutions from EMD Millipore (Billerica, MA).

SAMPLE PREPARATION FOR AFM OBSERVATIONS

Atomic Force Microscopy (AFM) samples were prepared as follows: 20~40μL of each solution was pipetted onto a freshly cleaved surface of SP-1 Grade highly-oriented pyrolytic graphite (HOPG) purchased from Structure Probe, Inc (West Chester, PA). The aqueous peptide solution was left to incubate for one hour at room temperature in an enclosed hydration chamber

(to prevent evaporation). The bulk of the solution was then removed by wicking with a laboratory tissue, followed by blowing with dry nitrogen for 30 seconds.

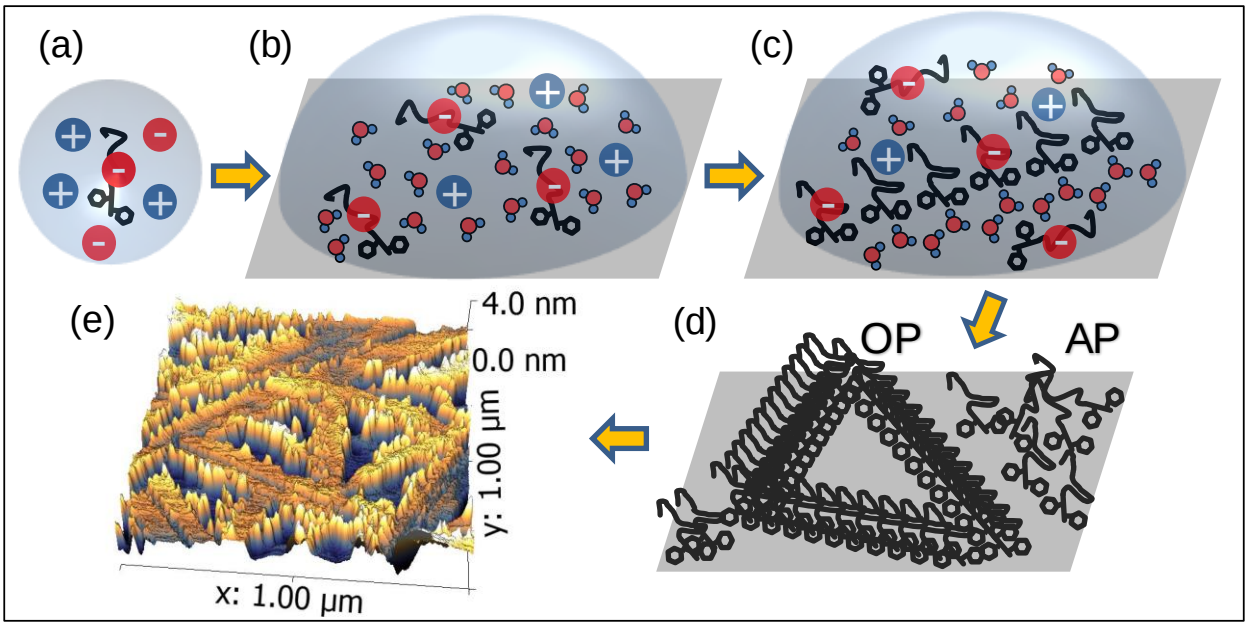

Figure 10: The method for preparing self-assembled peptide monolayers on graphite is outlined as follows: (a) Peptide solution is mixed with electrolyte of desired concentration; (b) A droplet of peptide/electrolyte solution is applied to the surface of HOPG; (c) The solution is held in an enclosed chamber to prevent evaporation as the peptides organize on the surface for 1 hour; (d) The water droplet is removed by wicking, followed by blow drying with nitrogen; (e) The surface topography is scanned by AFM.

Atomic Force Microscopy

Peptide nanostructures on HOPG were scanned by AFM, using either an Agilent 5500 AFM (Santa Clara, CA) equipped with an AC Mode III Module or a Digital Instruments (Veeco, Santa Barbara, CA) Multimode Nanoscope IIIa scanning probe microscope. High-frequency, aluminum-reflex-coated noncontact probes (125µm, 40N/m, 300kHz, r<10nm) were purchased from NanoAndMore USA (Lady's Island, SC) or NanoScience Instruments (Phoenix, AZ), and scanned in tapping mode with a set-point voltage of 2~4V.

DATA PROCESSING AND COVERAGE DETERMINATION

The acquired AFM images were analyzed using Gwyddion™ (http://gwyddion.net/) by performing operations such as mean plane subtraction, line-by-line height median matching, and Gaussian filtering to remove the underlying topography and emphasize the peptide structure.

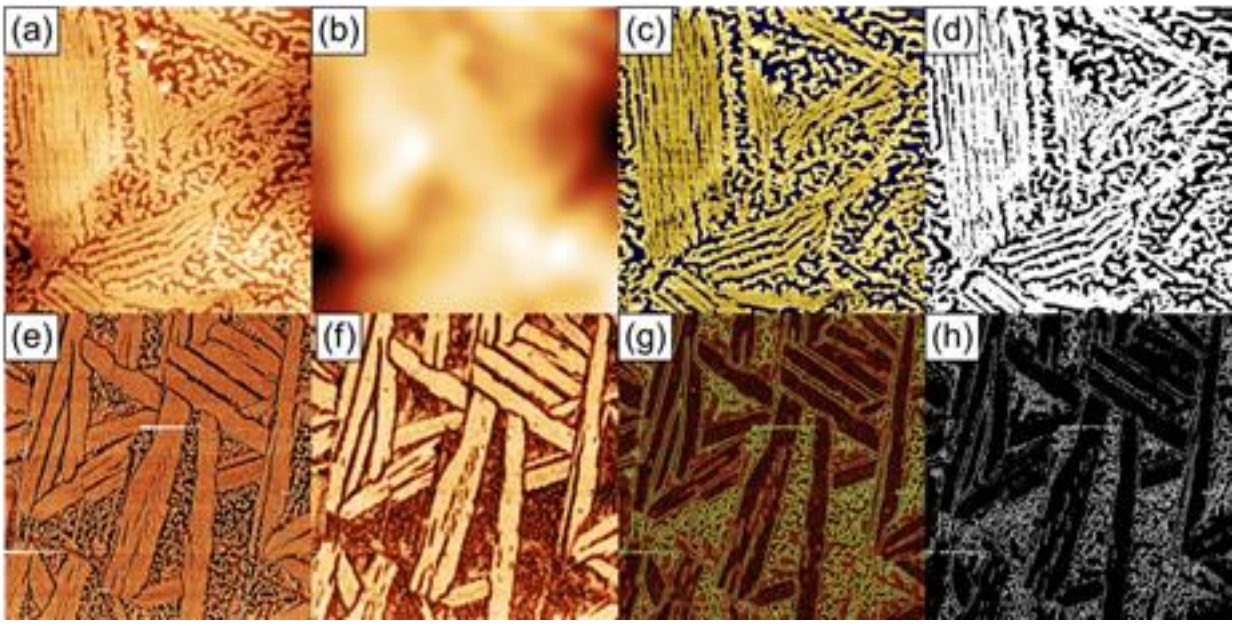

Figure 11: Measuring Peptide coverage by AFM image analysis. (a) Raw AFM image (b) Smooth out features to isolate background topography (c) Subtract background to isolate peptide structure (d) Measure total peptide coverage by planar threshold mask (e) Capture AFM phase image image (f) 5~10 pixel erosion filter to remove high spatial frequency features (g) Subtract low spatial frequency features from original image to isolate amorphous peptide structures (h) Measure percent coverage of amorphous peptide by planar threshold mask

IDENTIFICATION OF ORDERED (OP) VS. AMORPHOUS PHASE (AP)

Special care was taken to distinguish between the crystalline regions (ordered phase, OP) and the disordered regions (amorphous phase, AP) of the assembled peptides in each sample. The following defining characteristics were used to characterize the ordered phase: (i) Straight peptide nanowires or wider strips growing on six-fold symmetrical orientations on graphite (or graphene) surface (also visible as a 6-pointed star in the Fast Fourier Transform insets), (ii) The relative lack of surface roughness, and (iii) A slightly lower height profile than the amorphous phase, i.e., 1.8 nm vs 2.1 nm (see the height profiles below each image). Surface coverage data

was obtained from each processed image through the use of a planar threshold mask of the isolated peptide structure. The fractional surface coverage of OP vs. AP peptide was averaged over a series of 1x1μm~5x5μm AFM images of 2~6 separate samples in each condition, and the results were plotted against phosphate buffer concentration for each peptide. This procedure was repeated for GrBP5-WT and -M9 in 1mM H_3PO_4 and NaOH. The total peptide coverage was again broken down into fractions of OP and AP, and the results are shown for each electrolyte.

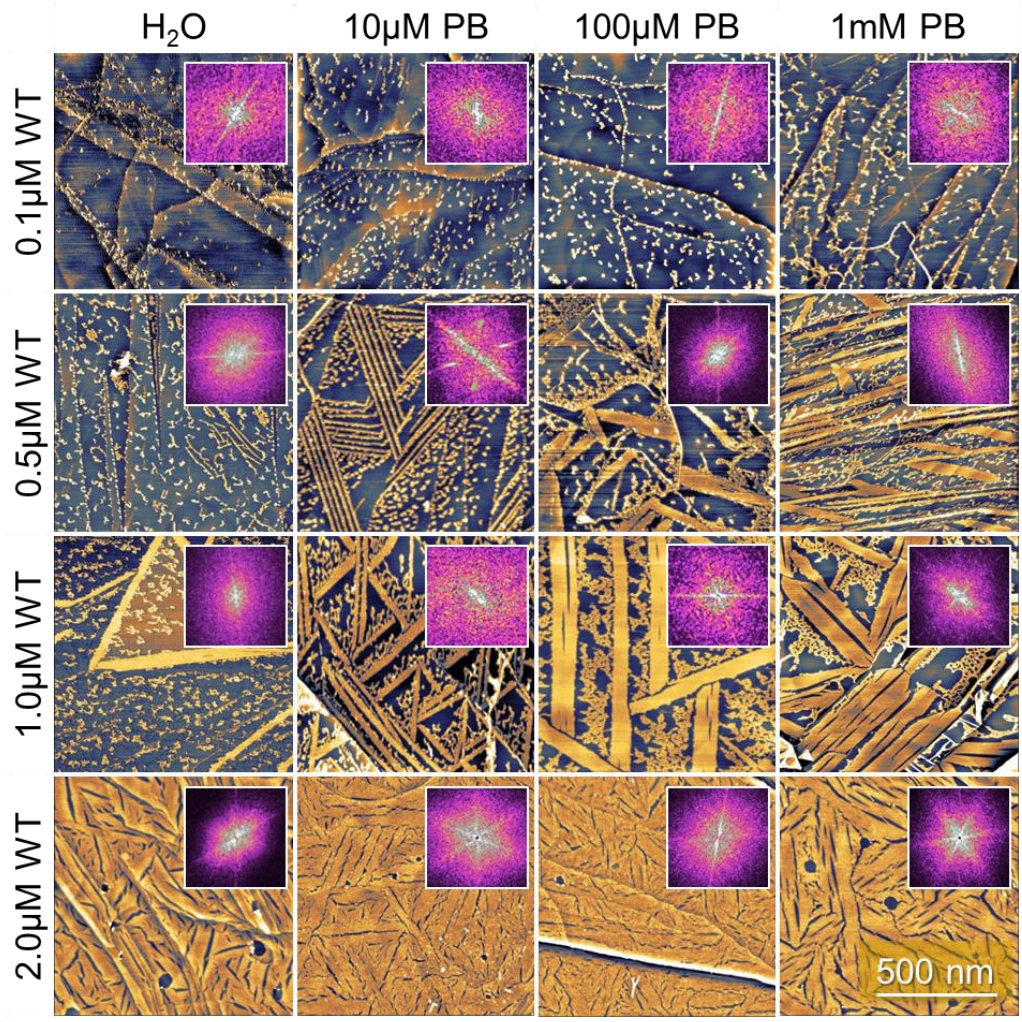

Figure 12: AFM of GrBP5-WT Self-Assembly on HOPG. AFM images of self-assembled peptide monolayers formed in varying concentrations of GrBP5-WT peptide (0.1μM, 0.5μM, 1.0μM, and 2.0μM) and electrolyte (DI water, and 10μM~1000μM sodium phosphate). All samples were incubated for 1 hour on HOPG. The Fast Fourier Transform (FFT) is inset into the upper right corner of each image to show the degree of symmetry in the ordered peptide nanostructures.

GRAPHITE DISPERSIONS

Aqueous graphite powder dispersions were prepared in solutions of GrBP5-WT, GrBP5-M9, and a control with no surfactant. 25mg of graphite powder (Asbury Graphite Mills, Warren County, NJ) was sonicated in 50mL of DI water for 30 minutes in a Branson Sonifier 250 (Branson Ultrasonics, Danbury, CT) set at 150 Watts (60% duty cycle) in a 26°C continuous flow water bath. This dispersion was centrifuged at low power (3500RPM) for 5 minutes to remove the largest graphite flakes, resulting in a drop in the area averaged particle diameter in the supernatant from 55µm to 20µm. Concentrated stock solutions (50~100µM) of GrBP5-WT or GrBP5-M9 were then added, to bring the final surfactant concentration to 8µM in four separate dispersions. Each of these dispersions was centrifuged an additional 5 minutes at 3500RPM to remove any graphite flakes which may have aggregated in the meantime. The supernatant then placed in a low-powered bath sonicator for 20 minutes to allow the peptide to absorb to the surface. Finally, 20µL of 100mM NaOH, NaH_2PO_4, or H_3PO_4 was added to 1.98mL of graphite-in-surfactant dispersion, to bring the total electrolyte concentration to 1mM in each 2mL cuvette. This moderate ionic strength allowed for application of the Smoluchowski approximation for electrophoretic mobility of colloidal particles, and calculation of the zeta potential. [22]

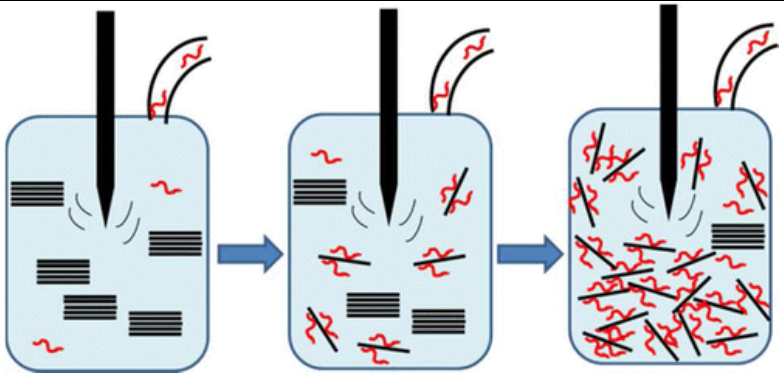

Figure 13: Notely *et al*, "Highly Concentrated Aqueous Suspensions of Graphene through Ultrasonic Exfoliation with Continuous Surfactant Addition", *Langmuir*, 2012 [23]

Zeta Potential Measurements

Immediately after preparation, each cuvette was placed in a ZetaPALS Zeta Potential Analyzer (Brookhaven Instruments, Holtsville, NY), and the electrophoretic mobility was measured by Phase-difference Laser Doppler Electrophoresis. The zeta potential was calculated for each sample, based on the average of 4 successive sets of 4 measurements (16 total) over the course of 15 minutes. The resulting zeta potential was compared with pH for each surfactant to establish the pH-dependent surface charge. [24]

Results

AFM Imaging Study of Buffer Effect

As described in the methods, all AFM samples were prepared from aqueous peptide solutions incubated for 1 hour at room temperature on HOPG, then dried and imaged by AFM. Several trends can be seen in the AFM images of GrBP5-WT on HOPG formed by solutions of varying peptide and sodium phosphate concentration. For each sodium phosphate concentration, the peptide coverage increased as the peptide concentration increased from 0.1μM to 2μM. For low peptide concentration (0.1μM), the overall coverage is low and only small clusters of peptides can be seen. Increasing the sodium phosphate concentration had little effect on this low peptide concentration. For high peptide concentration (2μM), the surface is completely covered by peptide, and changing the sodium phosphate concentration again had little effect. For 0.5μM and 1μM peptide concentrations, the peptide coverage significantly increased as the sodium phosphate concentration increased.

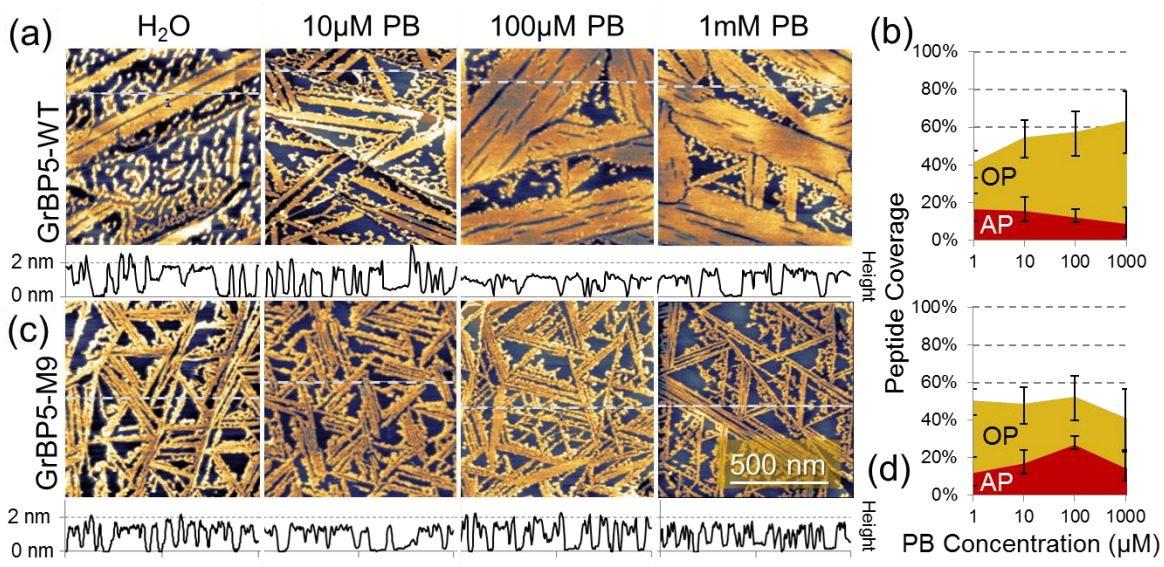

Figure 14: Surface Coverage and Morphology vs Electrolyte Concentration for WT and M9. AFM images of self-assembled monolayers formed by 1μM solutions of (a) GrBP5-WT and (b) GrBP5-M9 in varying electrolyte concentration (DI water, 10μM~1000μM sodium phosphate). All samples were incubated for 1 hour on freshly cleaved HOPG. Height profiles along the specified dotted lines are shown below each image, with a vertical sale of 2nm. The average surface coverage is plotted against phosphate buffer concentration for (c) GrBP5-WT and (d) GrBP5-M9. Error bars indicate standard deviation in surface coverage from 2~6 different samples. Total surface coverage is broken down into fractions of amorphous phase (AP) and ordered phase (OP).

A new set of samples were prepared from 1μM solutions of GrBP5-WT and -M9. The resulting structures were analyzed by considering two different measures: (i) Total surface coverage, and (ii) Morphology, which distinguished between crystalline (ordered, OP) and amorphous (disordered, AP) phases. The total surface coverage of GrBP5-WT increased from 40% to 65% as sodium phosphate buffer concentration increased from 0μM to 1μM (pH 4.1~5.8). At the same time, the fraction of crystalline phase, as well the crystalline domain size, increased at the expense of amorphous phase. In contrast, the non-charged mutant GrBP5-M9, showed a mix of thin crystalline nanowires and amorphous clusters, which remained largely unchanged as the buffer concentration increased.

Effect of pH

We next examined the effect of pH by dissolving each peptide in three separate 1mM electrolyte solutions: H_3PO_4 (pH 3.0~3.1), NaH_2PO_4 (pH 5.2~6.6), and NaOH (pH 7.3~10.4). Comparing GrBP5-WT assembled in H_3PO_4 and NaH_2PO_4, similar overall coverage is observed (55%, 65%, respectively), with the majority in the ordered phase (OP). In contrast, GrBP5-WT assembled in NaOH had surface coverage of only 20%, all in the amorphous phase (AP). The mutant M9 assembled into a nearly identical combination of crystalline nanowires and amorphous clusters in all three electrolytes.

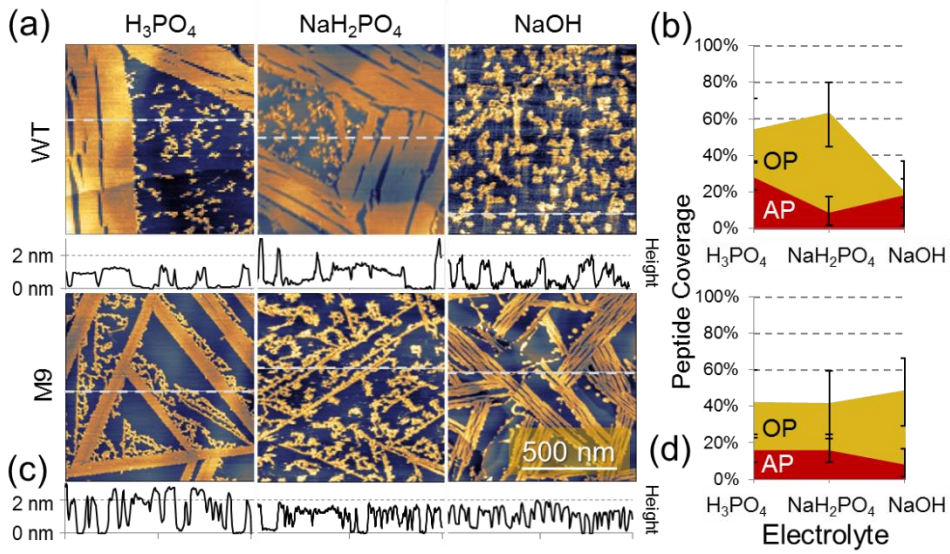

Figure 15: Surface Coverage and Morphology vs pH for WT and M9. AFM images of self-assembled monolayers formed by 1μM solutions of (a) GrBP5-WT and (b) GrBP5-M9 in varying electrolytes (with constant 1mM concentration): H_3PO_4, NaH_2PO_4, and NaOH. Height profiles along the specified dotted lines are shown below each image, with a vertical sale of 2nm. The plot of the surface coverage of (c) GrBP5-WT, and (d) GrBP5-M9 in each electrolyte is broken down into fractions of amorphous phase (AP) and ordered phase (OP). Error bars indicate the standard deviation in surface coverage from 2~6 different samples in each condition.

Graphite Zeta Potential

We next measured the electrophoretic mobility of aqueous graphite powder dispersions with and without peptide to determine the effect of peptide on the zeta potential. As described in the methods section, 1mM electrolytes (H_3PO_4, NaH_2PO_4, or NaOH) were to control the pH of each

of the dispersions. For graphite dispersed without surfactant, the zeta potential went from 0mV in H_3PO_4 to -37mV in NaH_2PO_4, and -49mV in NaOH. A similar trend (to varying degree) was observed in all samples (with or without peptide).

In order to isolate the effects of peptides on the surface charge, the "net" zeta potential of each peptide was calculated by subtracting the zeta potential of graphite alone from the zeta potential of graphite incubated with peptide at each pH. In H_3PO_4, both peptides induced a net positive zeta potential: +12mV (WT), and +17mV (M9). In NaH_2PO_4, GrBP5-WT contributed a moderate negative "net" zeta potential (-9mV), while GrBP5-M9 induced little change (-1mV). In NaOH, the WT peptide induced a somewhat more negative "net" zeta potential (-15mV), while the M9 peptide again had a negligible contribution (-2mV).

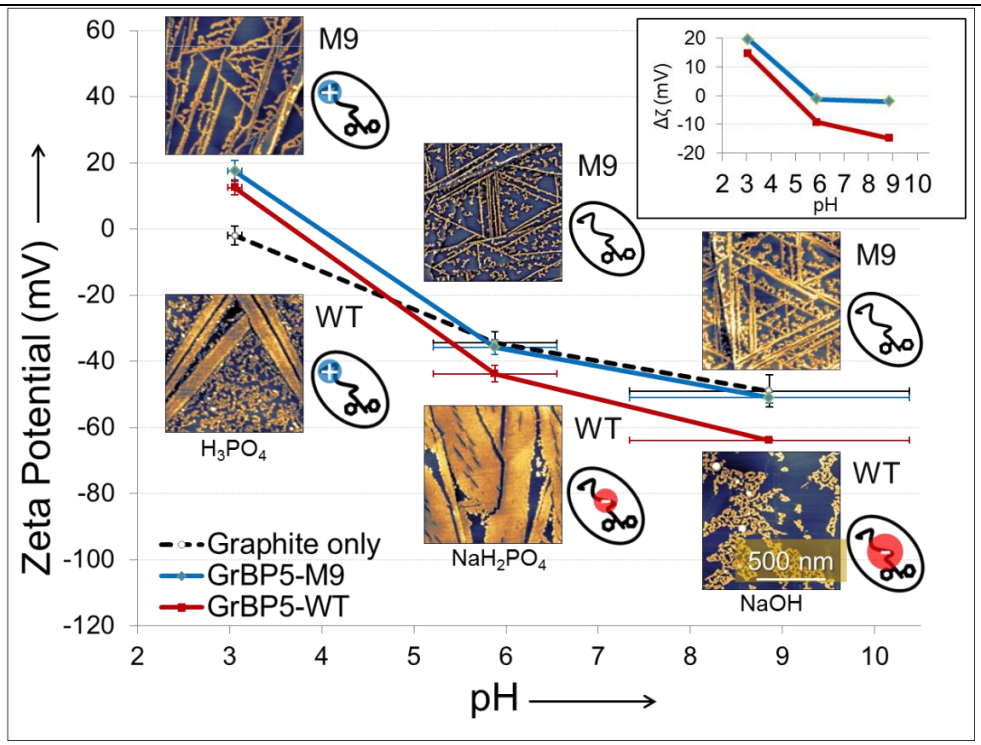

Figure 16: Zeta-potential of graphite dispersed in aqueous surfactant solutions is shown as a function of solution pH. Vertical error bars indicate the standard deviation in the zeta potential measurement of each sample, while horizontal error bars indicate the standard deviation in measurements of sample pH. 1x1µm AFM images of the corresponding surface morphology are shown for comparison. The inset shows the relative zeta potential (Δζ, mV) at each pH. The predicted peptide charge at each pH is indicated by the stick-figure models of GrBP5-M9 and GrBP5-WT next to the AFM images.

SPECTROPHOTOMETRIC TITRATION VIA TYROSINE FLUORESCENCE

Additional experiments were performed to monitor the changes to peptide fluorescence in varying pH conditions. The fluorescence of tyrosine allows for probing of de-protonation at high pH. [25] It was established that the aromatic tyrosine residues in GrBP5-WT can absorb light in the near UV, with wavelengths ranging from 230nm~235nm and 255nm~285nm, leading to fluorescence emission peaks in the range of 230~255nm and 280~305nm. However, in basic pH, this fluorescence is quenched due to the de-protonation of the phenolic hydrogen in tyrosine. The roughly ~50% fluorescence intensity observed in 2.5mM NaOH (pH 10) is consistent with the expected pKa in this range. [26]

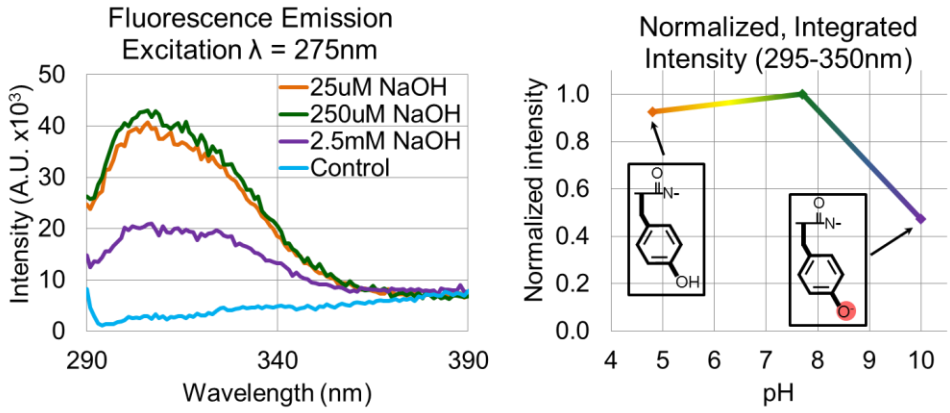

Figure 17: Fluorescence of GrBP5-WT in varying concentrations of NaOH.

DISCUSSION

The initial adsorption of low concentrations of GrBP5-WT on HOPG can be explained in terms of the hydrophobic effect. The hydrophobic effect is based on an entropic surface energy cost for any interface between a polar solvent (water) and non-polar surface (graphite), due to the formation of a semi-rigid hydration layer at the interface. The result is that any non-polar molecules will tend to adsorb to the interface, so as to require fewer water molecules to form a solvation shell. In the case of GrBP5-WT, this means that the hydrophobic domains of the

peptide (IMV, YSSY) will be tend to adsorb onto the hydrophobic graphite surface. An earlier study (So *et al*) [21] showed that the aromatic domain, in particular, is critical to the peptide's binding to graphite.

Increasing the peptide concentration, while holding the incubation time constant at 1 hour, led to an increase in surface coverage. When the peptide concentration reached a threshold surface density, a phase transition occurred on the graphite surface, similar to the formation of micelles in solution. Amorphous clusters gave way to crystalline nanowires, which tended to align along preferred orientations with six-fold rotational symmetry. This suggests a reduction in peptide-graphite surface energy depending on the orientation and folding pattern of the peptide, likely templated by the underlying graphite atomic lattice. A combination of polar (hydrophilic) and non-polar (hydrophobic) amino acids were found to be necessary to achieve these ordered structures by So *et al*.

When the ionic strength of the solution was increased up to 1mM with sodium phosphate, the surface coverage and crystallinity both increased, with the most dramatic effect observed for 1μM peptide. In contrast, the crystalline nanostructures formed by the peptide mutant M9 were largely unaffected by changes to the ionic strength. Thus, we demonstrated that the WT peptide's ionic strength sensitivity was primarily related to its two carboxylate residues, which can be explained by the ionic screening effect. That is, the close association of counter-ions around the negatively-charged peptide will decrease the intermolecular electrostatic repulsion.[27] In the case of M9, the ionic screening effect is negligible, since the acidic residues have been removed.

The effect of pH on the binding and morphology of these two peptides was also studied. Changing from 1mM NaH_2PO_4 (pH 5.2~6.6) to 1mM H_3PO_4 (pH 3.0~3.1) did not significantly

affect the binding or assembly of either peptide. In 1mM NaOH (pH 7.3~10.4), the M9 mutant was again largely unaffected, while the self-assembly of GrBP5-WT was disrupted.

Fluorescence measurements of GrBP5-WT in concentrated NaOH indicate that significant de-protonation of tyrosine occurs only above pH 9, which is beyond the pH range at which the peptide ordering breaks down. Thus, it is likely that the breakdown in ordering is related to the de-protonation of the carboxylic acid residues (4-glutamic acid and 7-aspartic acid), rather than the tyrosine residues. Although the expected pKa of glutamic acid and aspartic acid are 3.7 and 4.3, respectively, it is likely that the aggregation of peptides on the graphite surface stabilizes the acidic form of these residues. Zeta potential studies of ionic surfactant micelles (such as sodium dodecyl sulfate) have shown that when surfactant molecules are organized into micelles, the total micelle charge is typically only a fraction of the number of monomers in the micelle. [22] The moderate change to the negative zeta potential of graphite attributed to GrBP-WT in 1mM NaOH suggests that the carboxylic acid residues in this peptide are only partially deprotonated while adsorbed to the graphite surface. The fact that GrBP5-M9 had minimal effect on the zeta potential in NaOH confirms the connection between negative charge of GrBP5-WT and its carboxylic acid residues. However, both GrBP5-WT and -M9 contributed a net positive zeta potential to graphite dispersed in (acidic) 1mM H_3PO_4. This is most likely caused by the (partial) protonation of the C-terminus of both peptides, leaving a partial positive charge from the N-terminus. However, this did not seem to affect the peptide ordering observed by AFM.

CONCLUSION

In this study, we have demonstrated a convenient method to control the degree of crystallinity in self-assembled peptide-based biomolecular films on graphite by changing the ionic strength of the solution. We further showed that, *via* a simple mutation, the peptide can be changed from

being pH-sensitive to being pH-immune. Thus, the zwitterionic peptide surfactant, GrBP5-M9, can self-assemble into long-range ordered nanostructures on the surface of cleaved, atomically flat graphite over a wide pH range, from 3 to 10. This could prove useful in improving the robustness of self-assembled peptide monolayers, allowing them to tolerate the varying pH of different biological samples (blood serum, urine, and saliva) for better biomimetic sensor design. [28]

The negative charge of WT peptide adsorbed on graphite could also provide a useful avenue to stabilize aqueous colloidal dispersions of graphene. This has potential applications for inkjet printing of graphene or other layered materials, [23] or for preparation of solution-processed sprayed graphene field effect transistors. [29] Finally, this study further improves our understanding of peptide self-assembly on solid surfaces in varying pH and ionic strength, which can aid in investigations of other biologically significant ordered peptides (such as Huntington's, Alzheimer's, and Parkinson's amyloids), all significant in neurodegenerative diseases. [30]

PROPOSALS FOR FURTHER AREAS OF INVESTIGATION

COMPUTATIONAL MODELLING OF INTER-PEPTIDE INTERACTIONS ON 2D SOLID SURFACES

OBJECTIVE

In this study, we aim to investigate the aggregation of a graphite binding peptides on the surface of graphene, and characterize the intermolecular interaction of peptide side-chains leading to cluster formation using all-atom molecular dynamics simulations.

METHODS

For these simulations, we used the *in lucem* molecular mechanics package (based on the ENCAD force field) [31, 32] to calculated the forces on each atom from neighbors within 10Å. At 2fs intervals, we calculated the resulting changes to velocity and position of each particle to

predict a trajectory over simulation times ranging from 10~60ns. Initially, a single GrBP5-WT peptide model was inserted into a 10nm x 10nm x 10nm box with period boundary conditions, and the box was populated with simulated water molecules. Each water molecule was assigned a randomized initial position and velocity such that the overall average kinetic energy and density matched that predicted by the canonical model for 298K. Then, peptide molecule was allowed to relax in this environment for 50ns to determine a "solvated" molecular conformation. Then, starting from this configuration, a 5nm x 5nm graphene sheet was inserted into the simulation, starting at a distance of 8A from the peptide. The simulation was then run for another 50ns, as the peptide spontaneously adsorbed to the graphene surface.

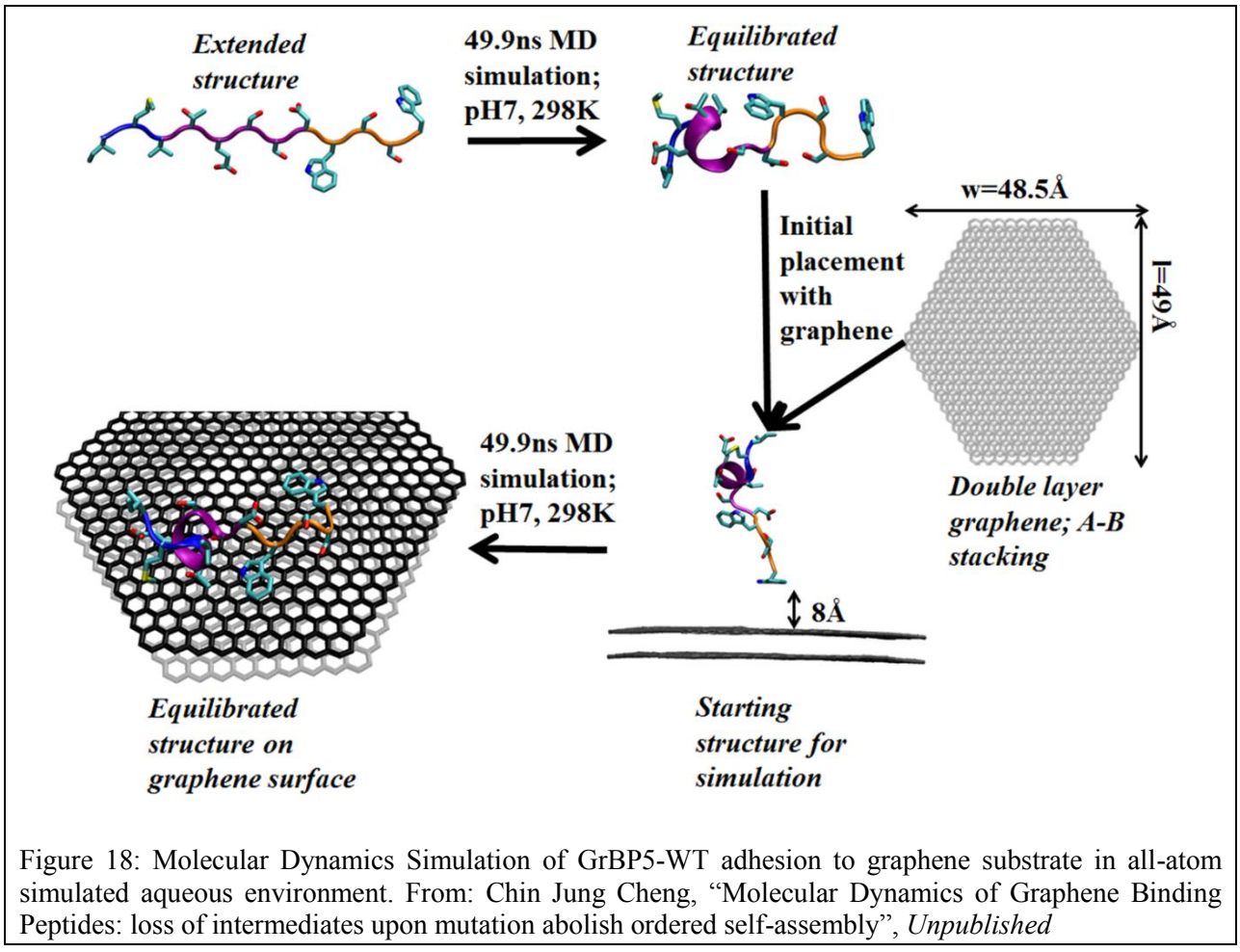

Figure 18: Molecular Dynamics Simulation of GrBP5-WT adhesion to graphene substrate in all-atom simulated aqueous environment. From: Chin Jung Cheng, "Molecular Dynamics of Graphene Binding Peptides: loss of intermediates upon mutation abolish ordered self-assembly", *Unpublished*

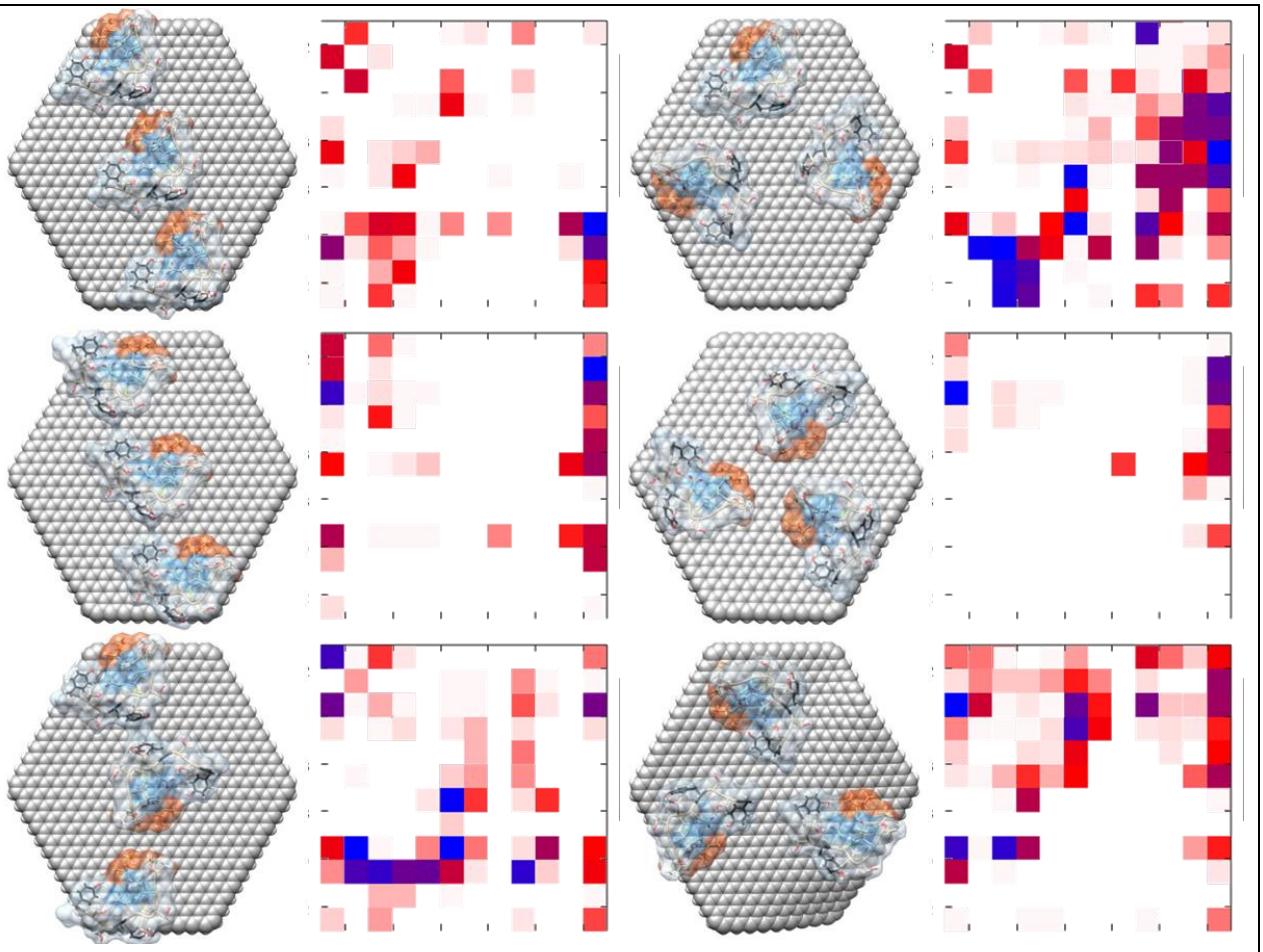

Figure 19: Inter-peptide contact maps corresponding to each simulation. Each box in the contact map corresponds to the total (normalized) contact time between specific side-chains in two adjacent peptides. The first row and column corresponds with the N-terminal Isoleucine residue, and the last row and column corresponds with the C-terminal tyrosine residue.

Starting from this surface-adsorbed configuration, two additional copies of the peptide molecule were added in six different arrangements on the graphene surface. This provided a survey of multiple different orientations in which two peptides could interact on the surface. Furthermore, each of these six starting configurations was run in three independent simulations, for a total of 18 simulations each run for at least 10ns. For each simulation, a contact map was generated which shows the amount of simulation time that a given residue from one peptide spends in contact with a given residue from another peptide. This includes side-chain side-chain, side-chain main-chain, and main-chain main-chain contacts. These total interaction times were

added together, and then normalized with respect to the longest overall contact time between any two residues in the simulation (to give values between 0 and 1). This gives a profile of the most common inter-peptide interactions, which may depend on that initial configuration. In addition, the contact time between the peptide side-chains and the graphene surface was also tracked, indicating which amino acids had the longest contact with the graphene surface.

RESULTS

In regards to the peptide-surface interactions, most of the simulations were quite consistent. Every simulation showed constant contact between 1-ILE and the graphene surface, as well as nearly constant contact with 2-MET and slightly weaker contact with 3-VAL. All of the simulations show a lot of contact with 9-TYR and 12-TYR. All other residues showed essentially zero contact with the surface, with the exception of some intermittent contact with 8-ASP and and 9-SER. In addition, an extensive intramolecular hydrogen bonding network seems to hold each peptide in a remarkably steady conformation. This network seems to be centered around 5-GLU, which forms hydrogen bonds with 4-THR along with the N-terminus and backbone NH group of 1-ILE.

While there was substantial diversity in the inter-peptide contact-maps from the 18 different simulation runs, certain residue interaction pairs seemed to occur frequently. The most commonly observed inter-peptide interaction was the clustering of hydrophobic residues 1-ILE and 3-VAL. This seemed to be a common initial contact point, and was often the longest contact in the simulation. Occasional intermolecular hydrogen bonds were also observed, such as between 6-SER and 4-THR or between the OH group of 9-TYR and the backbone oxygen of 6-GLU.

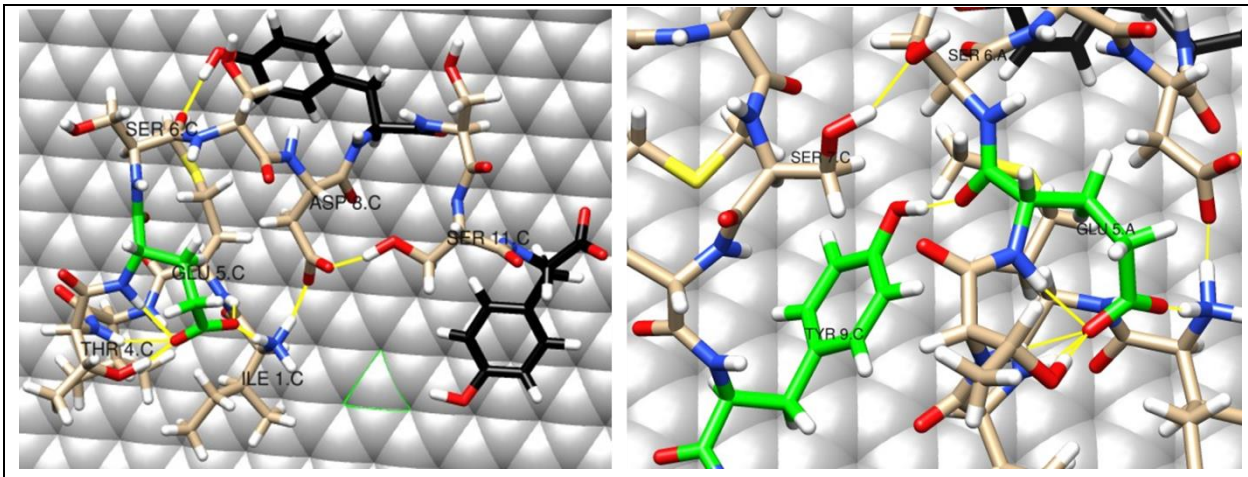

Figure 20: Close-up of GrBP5-WT on graphene, showing intramolecular hydrogen bonding network (left) and inter-molecular hydrogen bonding (right).

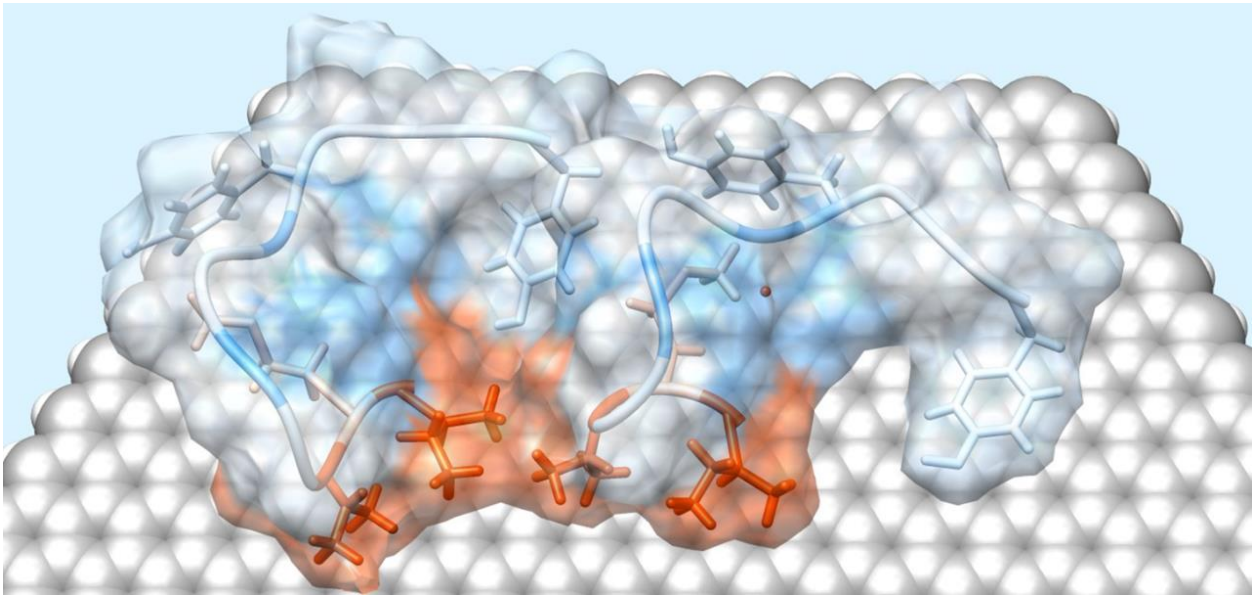

Figure 21: Molecular Dynamics Simulation of two peptides interacting on graphene, highlighting hydrophobicity surface. Orange = Hydrophobic, Blue = Hydrophilic.

DISCUSSION

This simulation confirmed that tyrosine plays a major role in the adsorption of GrBP5-WT to the graphene surface. The two tyrosine residues were not only the first to contact the surface, but they remained in contact throughout the duration of the simulation. In addition, it was found that the hydrophobic "head" domain (IMV) of the three peptide molecules also maintained contact with the graphene surface throughout the simulation. It also showed that the C-terminal tyrosine

residue, and the hydrophobic "head" at the N-terminus (IMV), also had the most intermolecular contact with the other peptides. The hydrophilic middle of the peptide (TESSD) had almost no contact with either the graphene surface or the neighboring peptides. This is likely because the polar residues are stabilized by the polar solvent (water). This is also consistent with the contact angle experiments, which indicate that, in situations with low overall surface coverage, peptide absorption to graphene tends to lower the water contact angle (indicating that the graphite surface becomes more polar, or hydrophilic). [33]

Using simulation we would like to have demonstrated the change in conformation from the "amorphous" to the "ordered" structures observed in experiment. However, in order to simulate this behavior, it is likely that we would need a considerably larger graphene surface, with many more peptide molecules. Experimental results indicate that long-range ordered-phase self-assembly requires the combined contribution of many small forces over a wide area, and that a particular "threshold" surface coverage is necessary in order for this transition to occur. For now this threshold is out of reach given the current limitations of computational resources.

Effects of Substrate on Self-Assembly of Peptides

CVD Graphene

In addition to the substrate material itself, differences in the substrate structure can also impact the resulting self-assembled peptide structure. In one such example, GrBP5-WT was shown to self-assemble into ordered nanostructures on CVD graphene grown on a copper foil. In this case, several different nanostructures were observed on different areas of the CVD graphene. It is hypothesized that these differences indicate that the peptide nanostructure is influenced by the sub-graphene copper crystal facets.

Chemical vapor deposition (CVD) is a method for preparing large-area, single-layer graphene films on a copper or nickel foil using a tube furnace with a methane-hydrogen-argon atmosphere.

[34, 35] Graphene formation can occur either through diffusion of carbon atoms through the metal at high temperatures, driven by the reduction of surface energy by the formation of graphene, or through the catalytic liberation of hydrogen from methane on the metal surface. The production of the copper foil involves rolling out thicker copper slabs, which leaves behind 100nm ridges due to the slipping of atomic planes from plastic deformation. Copper oxide is removed from the copper surface by annealing at 700~800°C prior to graphene deposition. This reduced copper surface is protected from later oxidation by the graphene layer, leaving intact the atomically flat copper crystal facets underneath the graphene. [36] In addition, grain boundaries in the original copper slab are preserved, leading to several possible crystallographic orientations exposed to the surface in different locations. However, detailed STM studies have revealed that the growth of large-area graphene films is largely unaffected by this different copper crystal facets. [37]

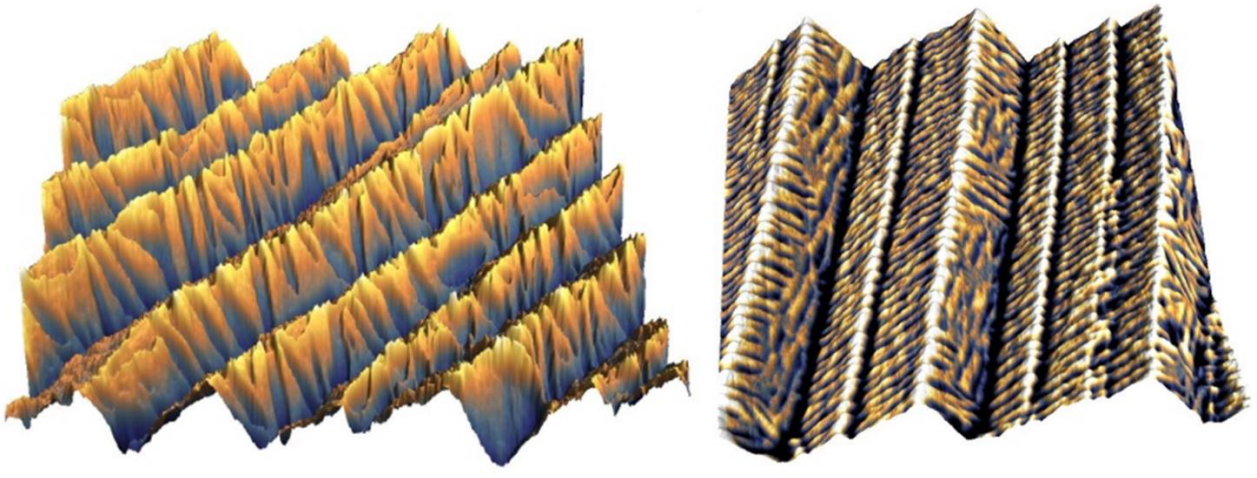

Figure 22: Peptide self-assembled structures on CVD graphene (3D projection)

If the peptide structure is examined near such a grain boundary, some variation in the peptide structure can be seen on either side of the grain boundary, supporting the idea that the sub-

surface copper crystal faces can affect the peptide structure. Further investigation will be necessary to elucidate this connection in detail.

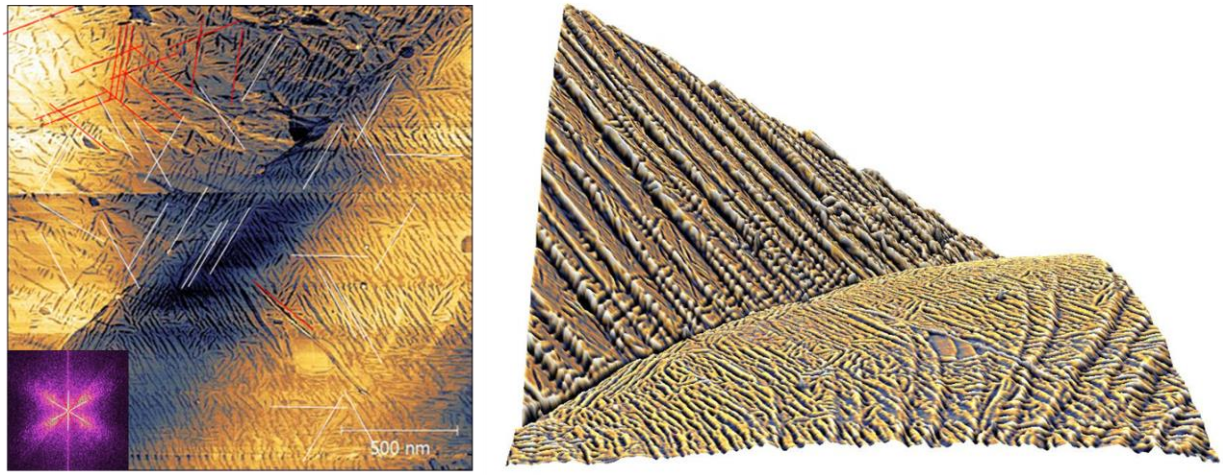

Figure 23: Effect of underlying copper grain boundaries on peptide structure assembled on CVD graphene.

EFFECT OF GRAPHITE STACKING FAULTS ON SELF-ASSEMBLED PEPTIDE STRUCTURE

GrBP5-WT incubated on exfoliated graphite flakes generally result in the same peptide structure as that seen on HOPG, in which many short (100~500nm) "nanowires" or "nano-tapes" are observed to criss-cross the surface. However, on some exfoliated graphite flakes, large domains of ordered peptide can be found, in which the peptide nanowires are all aligned in the same direction. Alternatively, "hybrid" structures can also be seen, with uniformly-aligned "domains" mixed with short "nano-tapes".

These ordered domains (both the large, parallel domains, and the criss-crossing nanowires) generally occur with 6-fold rotational symmetry, indicating that each domain is aligned to the graphite lattice in some way. Careful observation of the angle formed between the two distinct "hybrid" domains shows that they are almost, but not quite, perpendicular to each other. It remains an open question the cause of these different peptide nanostructures. One likely

explanation is the presence of stacking faults in the graphite, leading to a difference in the sub-surface crystal lattice.

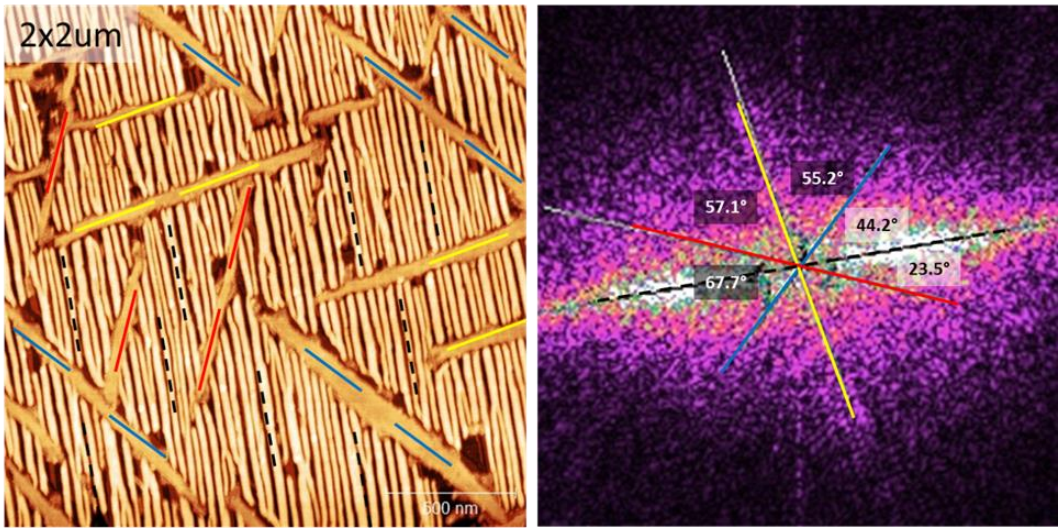

Figure 24: Hybrid peptide nanostructures on exfoliated graphite flakes, likely caused by stacking faults in graphite crystal.

OTHER LAYERED MATERIALS

Aside from graphene, there are a number of 6-fold symmetric, atomically flat layered substrate materials available, which can be exfoliated by similar means (mechanical exfoliation, chemical vapor deposition, sonication and colloidal dispersion).

Transition metal dichalcogenides, such as MoS_2, $MoSe_2$, WS_2, and WSe_2 have semiconducting properties with varying band-gaps in the visible-light range which can be useful for ultra-thin flexible transistor devices (including logic gates, LED's and photodiodes). [38-43] In addition, their high sensitivity to surface dopants could potentially lead to wireless biosensor devices based on photoluminescence rather than electrical conductivity. [44]

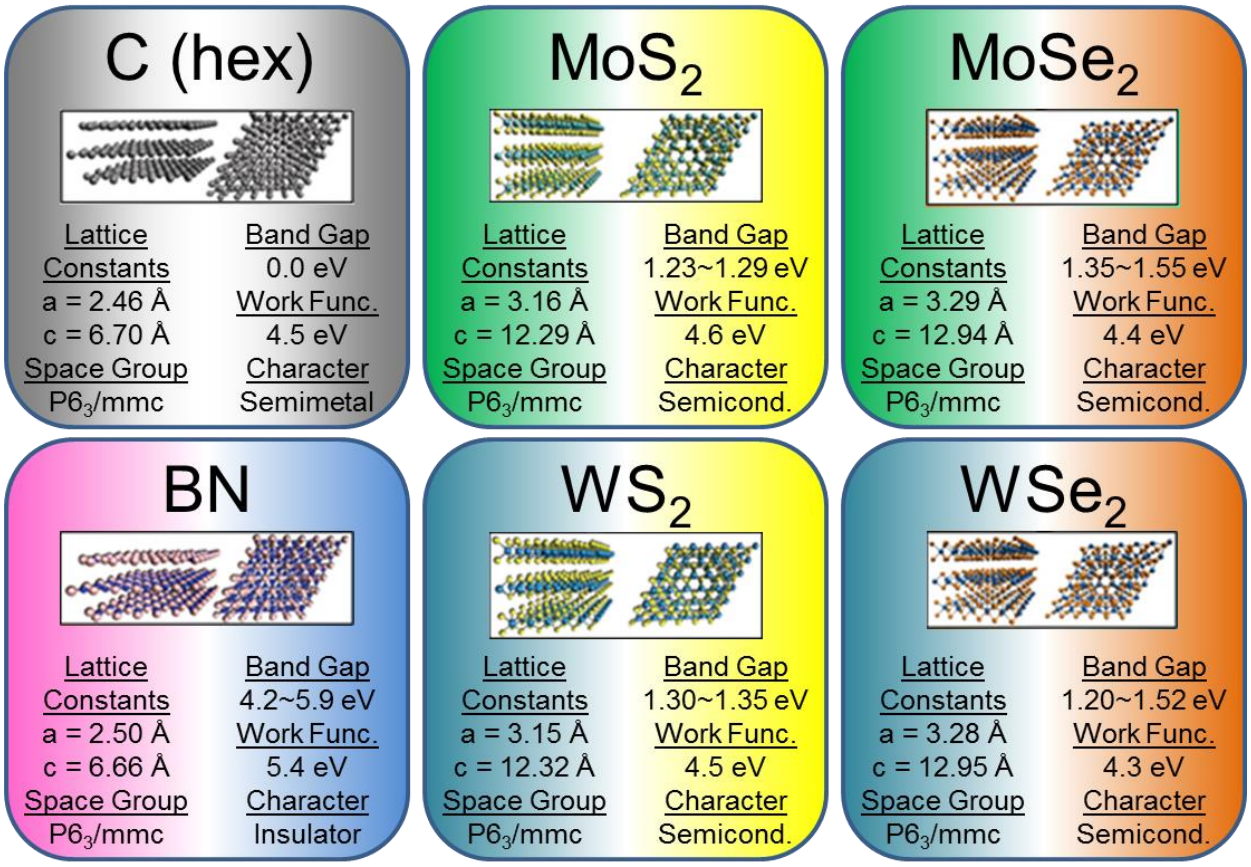

Figure 25: Properties of selected atomically flat layered materials, including lattice constants, crystal symmetry, band gap, work function, and electronic character.

Hexagonal boron nitride (h-BN) has a crystal structure nearly identical to graphene, but with the carbon atoms replaced by alternating boron and nitrogen atoms. This highly polar bond eliminates the conductivity found in graphene, resulting in an atomically flat, high-bandgap (5.4eV) insulating dielectric material. [45] Single- or few-layer h-BN has been used as a gate dielectric for highly efficient proof-of-concept graphene FET devices. [46] The ultra-thin dielectric allows for high capacitance, and the uniform, atomically flat structure leads to high mobility in the graphene channel.

BN substrates could also be useful to directly characterize the charge-transport properties of peptide monolayers themselves, in contrast with monolayers formed on graphene (which modify the conductivity of the substrate). Due to the lack of π-conjugation in the peptide backbone,

appreciable electrical conductivity is not expected. The most likely scenario would be some form of AC dissipation losses from water molecule dipole relaxation akin to the conductivity of DNA.[47] Alternatively, monolayers formed by a highly acidic peptide mutant may support conduction of protons, similarly to chitosan. [48]

GrBP5-WT, and two mutants (M6 and M8), have been shown to bind with high affinity, and form ordered structures, on each of these layered material (with some exceptions).

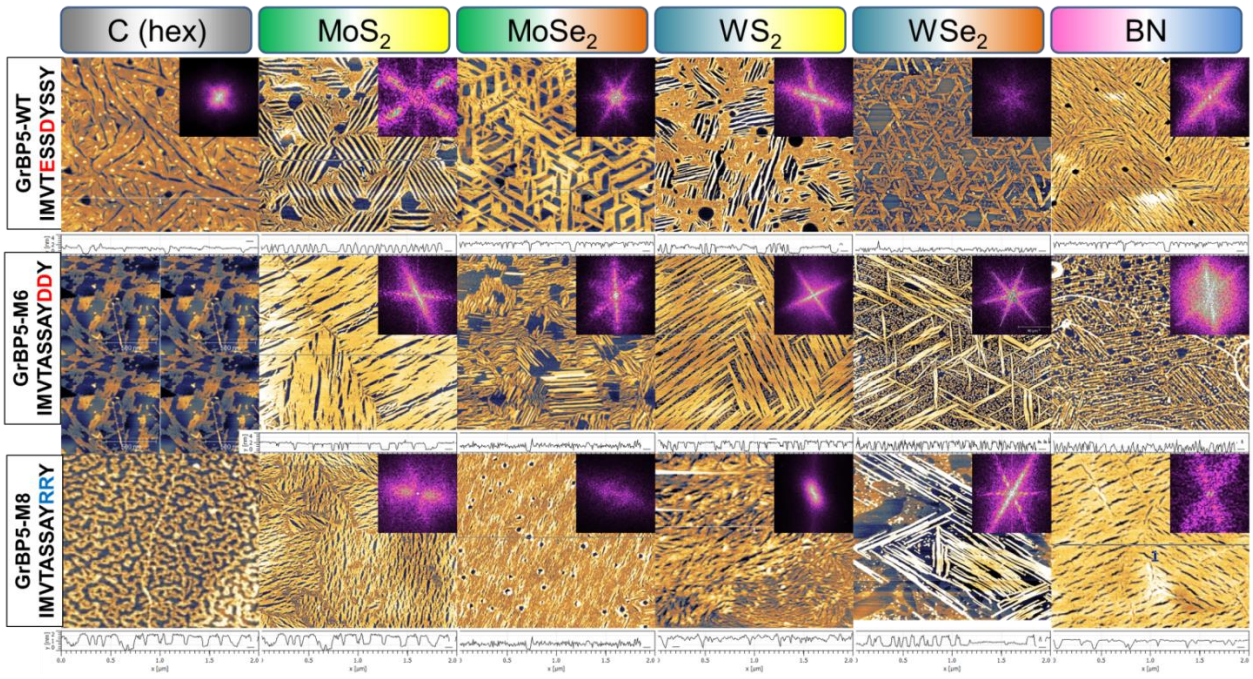

Figure 26: Peptide self-assembled nanostructures on selected atomically flat layered materials.

EFFECTS OF SURFACE CONTAMINATION

One of the challenges in forming self-assembled peptide nanostructures is the requirement for extremely pristine surfaces. Any wet chemistry processing or polymer coatings (such as PMMA) on atomically flat layered materials leaves behind a residue that can disrupt peptide ordering. No cleaning technique thus far tested has been able to restore a surface to the required pristine state to allow peptide self-assembly after a surface has been contaminated. This includes washing with acetone, IPA, ethanol and water, and/or annealing at 400°C in argon. The result is that

photolithography, electron beam lithography, and a variety of other transferring techniques (such as etching copper with nitric acid lifting off graphene with a polymer film) can present challenges, if ordered peptide nanostructures are required.

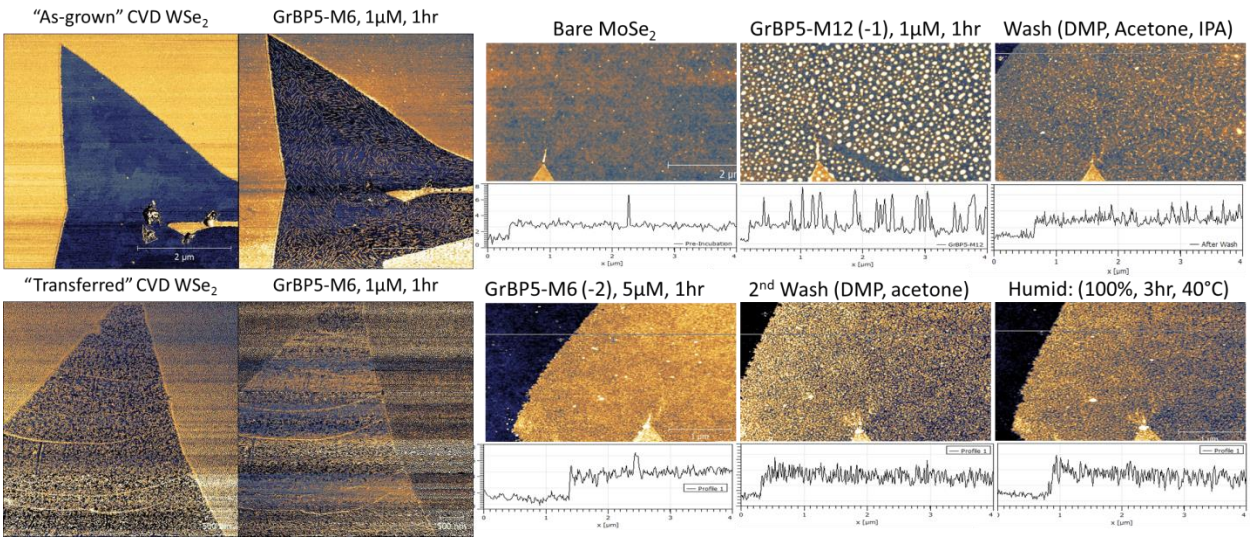

Figure 27: Effect of surface contamination on peptide self-assembly. Peptide self-assembly occurs readily on "as-grown" CVD WSe_2, but contamination by polycarbonate transfer polymer residue prevents peptide absorption and self-assembly. Attempts to wash away peptide with organic solvents (DMP, Acetone, IPA) were largely ineffective.

INDIUM MICROSOLDERING

For experiments which require electrodes to be applied (such as FET devices, photodiodes, etc.), indium microsoldering is an attractive method because it is not necessary to coat the surface with polymer. [49] In this procedure, the substrate is first heated to 180°C with a table-top heating element (enough to melt indium). A copper wire is attached to an xyz-microcontroller, and dipped into the molten indium. By slowly extracting the copper wire from the indium, a long thin tip is produced. Once a single-layered graphene crystal on SiO_2 is identified in the optical microscope, this indium tip is melted onto the edge of the graphene (still hot), and drawn into a wire.

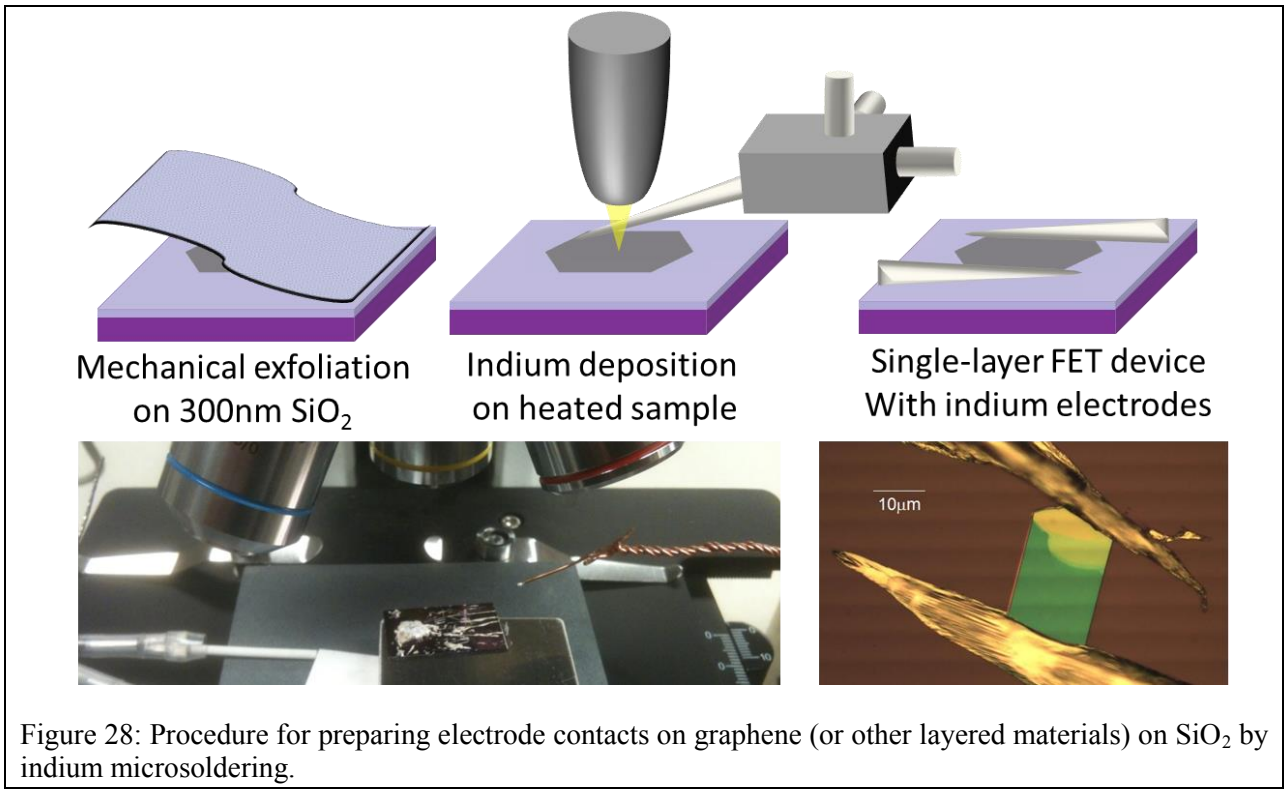

Figure 28: Procedure for preparing electrode contacts on graphene (or other layered materials) on SiO_2 by indium microsoldering.

TUNING THE OPTICAL PROPERTIES OF $MoSe_2$ BY PEPTIDE ADSORPTION

INTRODUCTION

$MoSe_2$ is layered semiconductor material which has an "indirect band-gap" of 1.35~1.55 eV in the bulk crystalline form. [43] An *indirect* band gap means that the smallest energy transition involves both a change in energy and in momentum, which requires simultaneous absorption of a photon and a phonon. Therefore, multilayered $MoSe_2$ has a low probability of electron transition, and thus a low quantum efficiency, and low fluorescence intensity. In single-layer form, $MoSe_2$ has a *direct* band-gap of 1.6 eV. A direct band gap means that the smallest energy transition from the valence band to the conduction band does not involve any change in momentum (occurring at the K-point of the Brillouin zone), so it has a much larger quantum efficiency and fluorescence intensity.

When a photon is absorbed by single-layer $MoSe_2$, a single electron is excited across the band gap into the conduction band, and a "hole" is left behind. This electron and hole have a lifetime

on the order of 126ps before annihilating and emitting a photon back out. [50] However, before annihilating, the two oppositely charged "particles" are attracted to each other by the Coulombic force, and form a transiently stable entity known as an exciton. Exciton formation leads to a moderate decrease in the energy of the electron-hole system, so the photon emitted upon annihilation will have lower energy than the band-gap energy. If the $MoSe_2$ crystal is heavily doped (charge imbalanced), excess electrons or holes will be attracted to these excitons, and form an entity known as a trion (e-e-h or e-h-h) due to Coulombic attraction of the free electron to the electron-hole pair. [51] This results in a further reduction in energy of the emitted photon upon annihilation. This property provides a means to detect the charge imbalance in single layered $MoSe_2$ using only optical measurements. However, this energy difference can only be detected at extremely low temperatures (25K), which requires the sample to be cooled by liquid helium in a vacuum chamber.

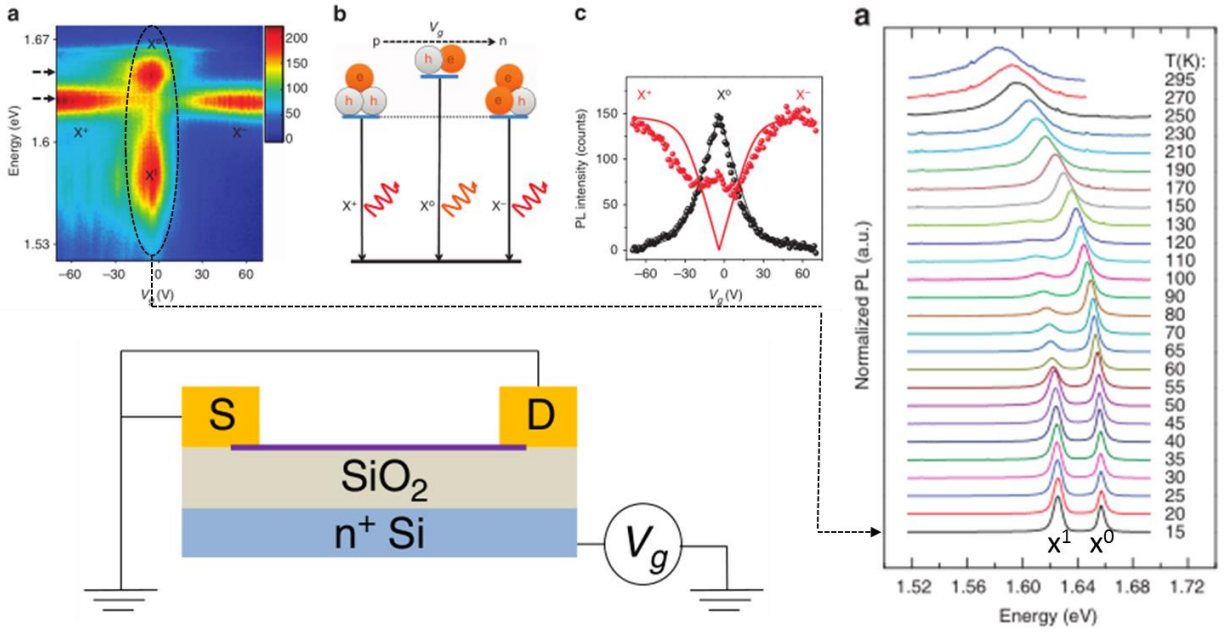

Figure 29: Effects of gate voltage and temperature on the photoluminescence of single-layer $MoSe_2$. Ross *et al*, "Electrical control of neutral and charged excitons in monolayer semiconductor" *Nature Communications*, 2013

The high surface-area to volume ratio makes single-layer $MoSe_2$ highly sensitive to "molecular doping" from absorbed species. This makes single-layer $MoSe_2$ well-suited to test the effects of peptide absorption, and could potentially lead to useful application as a biosensor.

In this study, we tested the effect of several mutant graphite-binding peptides on the photoluminescence of single-layer $MoSe_2$ crystals. Our hypothesis was that, by controlling the charge on the peptide, we could control the degree of doping of the $MoSe_2$ surface.

MATERIALS AND METHODS

Samples of $MoSe_2$ were prepared by mechanical exfoliation onto 300nm thermal SiO_2 on P-doped silicon wafers, similar to the method of preparing graphene. Five peptide mutants were tested, each with a different peptide charge: GrBP5-WT (IMVTESSDYSSY), -M6 (IMVTASSAYDDY), -M8 (IMVTASSAYRRY), -M11 (IMVTESSRYSSY), and -M12 (IMVTASSDYSSY). Two of the mutants contained two carboxylic acid side-chains, giving them a -2 charge (WT, M9), one mutant contained two amine side-chains, giving it a +2 charge (M8), one mutant contained both amine and carboxylic acid side-chains, giving it a net 0 charge (M11), and one had a single carboxylic acid side-chain, giving it a -1 charge (M12).

Once a suitable single-layered crystal was identified, it was incubated in a 1µM solution of peptide in DI water for 1 hour. This standard concentration and incubation time was selected to give an ideal moderate coverage of ordered peptide nanostructures, without completely saturating the surface. A lower concentration may lead to insufficient peptide coverage, with the peptide clustering into amorphous structures. A higher concentration may overcrowd the surface, leading to higher nucleation density of the ordered structures (and thus, shorter "nano-wires). The sample was then cooled by liquid helium to 25K, and the photoluminescence spectrum was measured.

In a separate experiment, a large, single-layered $MoSe_2$ crystal isolated on SiO_2, and an electrode contact was prepared by indium microsoldering. A separate contact was made directly to the P-doped silicon substrate, to act as a gate electrode. The sample was incubated in 1µM GrBP5 peptide as before. In this configuration, the photoluminescence at low temperature in vacuum could be examined as a function of gate voltage.

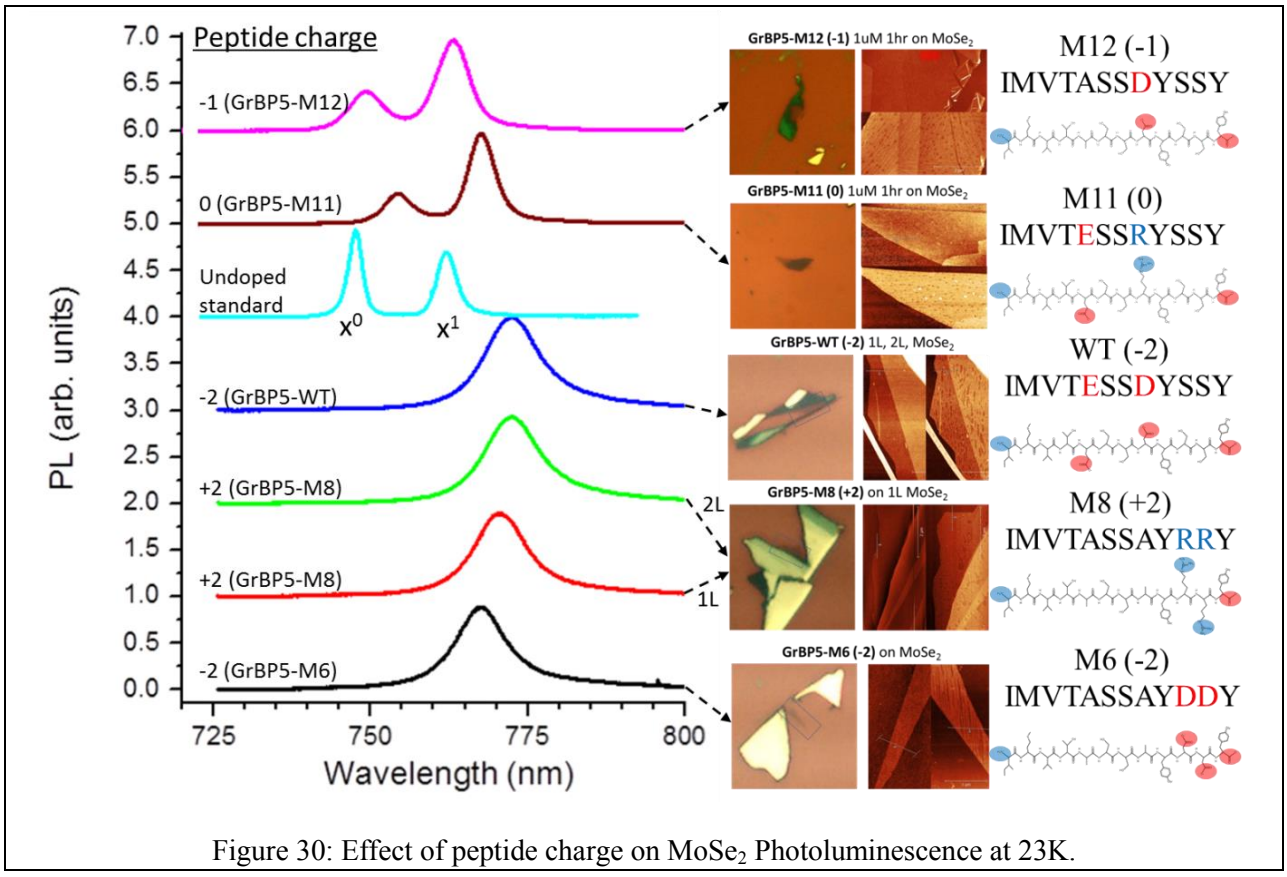

Figure 30: Effect of peptide charge on $MoSe_2$ Photoluminescence at 23K.

RESULTS AND DISCUSSION

The experimental results show a significant effect from peptide adsorption to the surface, as compared with the "un-doped standard". In the absence of doping, two peaks can be observed centered at 750nm and 763nm (1.57eV and 1.65eV). When the $MoSe_2$ is coated with either the negatively charged (WT, M6) or the positively charged (M8) mutant peptides, the original peaks are completely eliminated and replaced with a single peak centered around 1.63eV (755nm).

This peak is thought to correspond to the recombination of "charged excitons", or "trions", in $MoSe_2$. According to theoretical calculations, positively and negatively charged trions have the same energy, so it is expected that both positively and negatively charged peptides will produce the same observed effect. However, peptides with a lower (M12), or zero charge magnitude (M11) were used, the original "neutral exciton" photoluminescence signature was observed.

When a large negative gate voltage (-80V) was applied to a sample coated by GrBP5-M6, it was found that the original "un-doped" signature could be restored. Since a negative gate-voltage induced a positive charge in the $MoSe_2$ surface, this indicates that the peptide was causing N-doping to the $MoSe_2$.

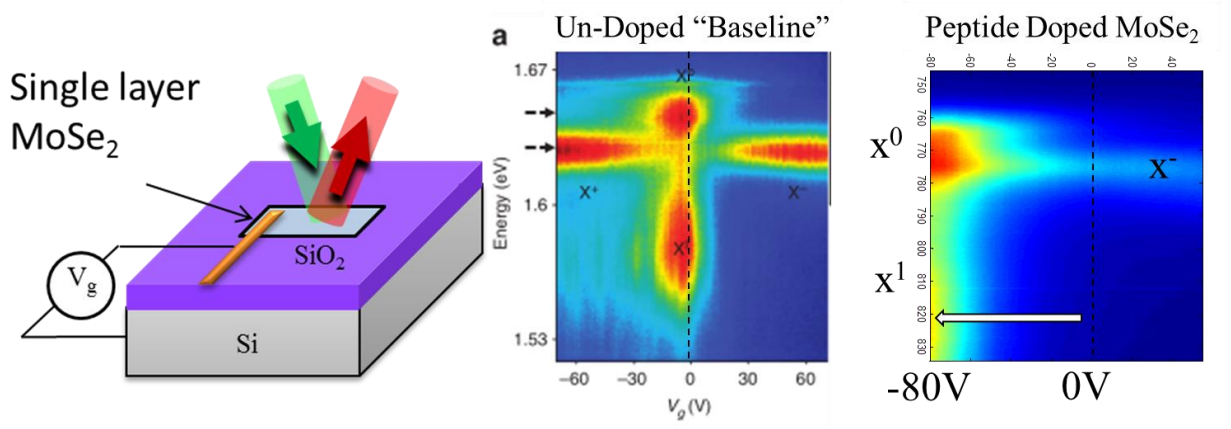

Figure 31: Doping effect of GrBP5-M6 (100nM, 10 min) on SL $MoSe_2$ PL at 23K, with varying back-gate voltage.

Creation of a Glucose Sensor or Biofuel Cell by Enzyme Immobilization

Immobilization of enzymes on solid surfaces is an ongoing challenge for a variety of application in bioelectronics. [1, 19, 52] Self-assembled solid-binding peptide monolayers offer a unique approach to solving this technological challenge due to their inherent biocompatibiltity, and adaptability to varying substrates. Glucose oxidase provides a model enzyme to demonstrate this capability, which can form the basis for a glucose biosensor device in the short term, and a bio-fuel cell system in the long term. By incorporating the enzyme cofactor NADH into the tail

of a graphite-binding peptide, we expect that glucose oxydase enzymes can be immobilized onto a graphene field effect transistor with high affinity and activity. With a height of ~1nm, this graphite-binding peptide linker should offer minimal resistance to the capture of electrons by the graphene channel.

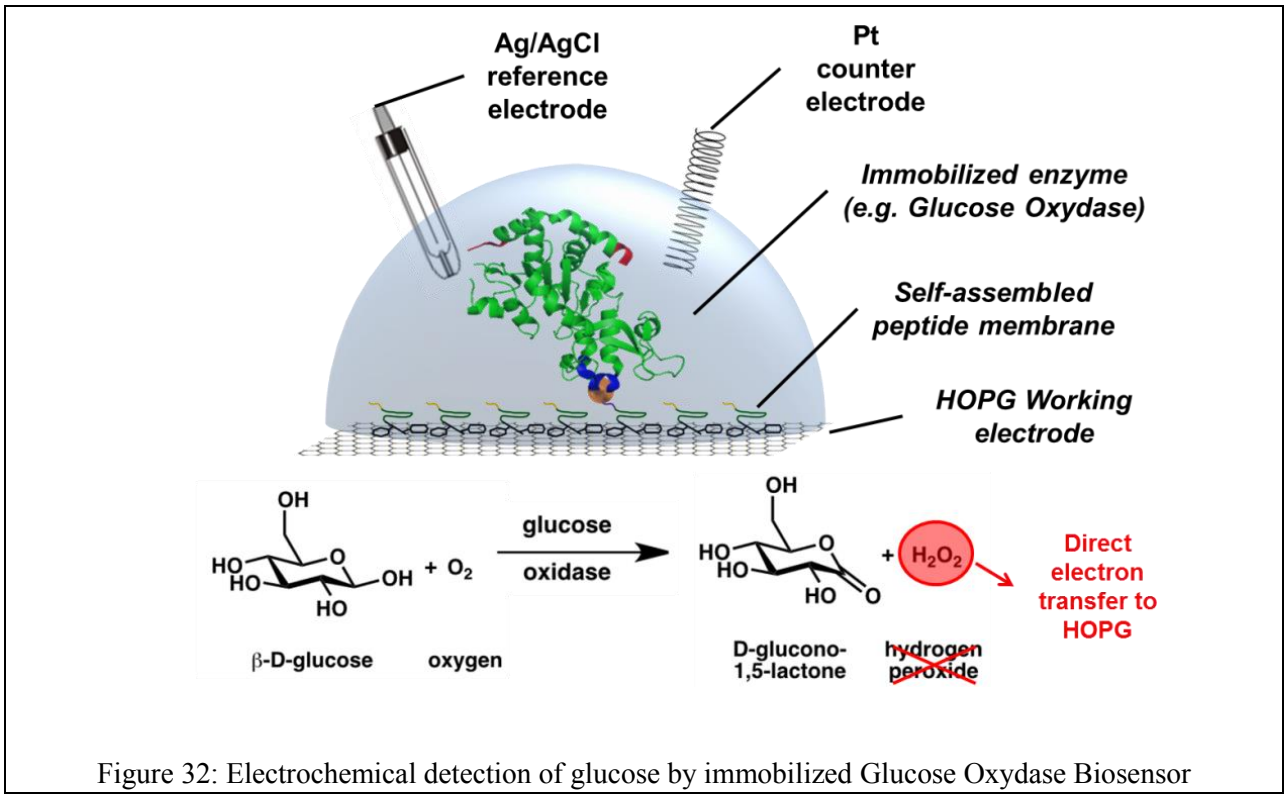

Figure 32: Electrochemical detection of glucose by immobilized Glucose Oxydase Biosensor

CONCLUSION

This work demonstrates the applicability of solid binding peptides to a variety of atomically flat 2D layered materials, and proposes possible applications in the field of biosensors and bio fuel cells. Several fundamental parameters affecting the process of peptide self-assembly on atomically flat layered materials were examined, including the effects of pH and electrolyte, peptide mutations, and changes to the substrate and sub-surface crystal structure and physical properties. Additionally, computational modelling was applied to better elucidate the role of

hydrophilic/hydrophobic properties and hydrogen bonding on the molecular conformation and intermolecular interactions of peptides on atomically flat solid surfaces.

Surface contamination by polymer and solvent residues were found to be detrimental to peptide self-assembly, and so the technique of indium microsoldering was proposed as a method to prepare electrical contacts for field-effect transistors while avoiding surface contamination. Finally, this knowledge was put to use in order to characterize the effects of peptide charge on the photoluminescence of single layered $MoSe_2$.

OUTLINE OF PROPOSED FUTURE WORK

David Starkebaum- Milestones towards PhD Completion; 2June2016

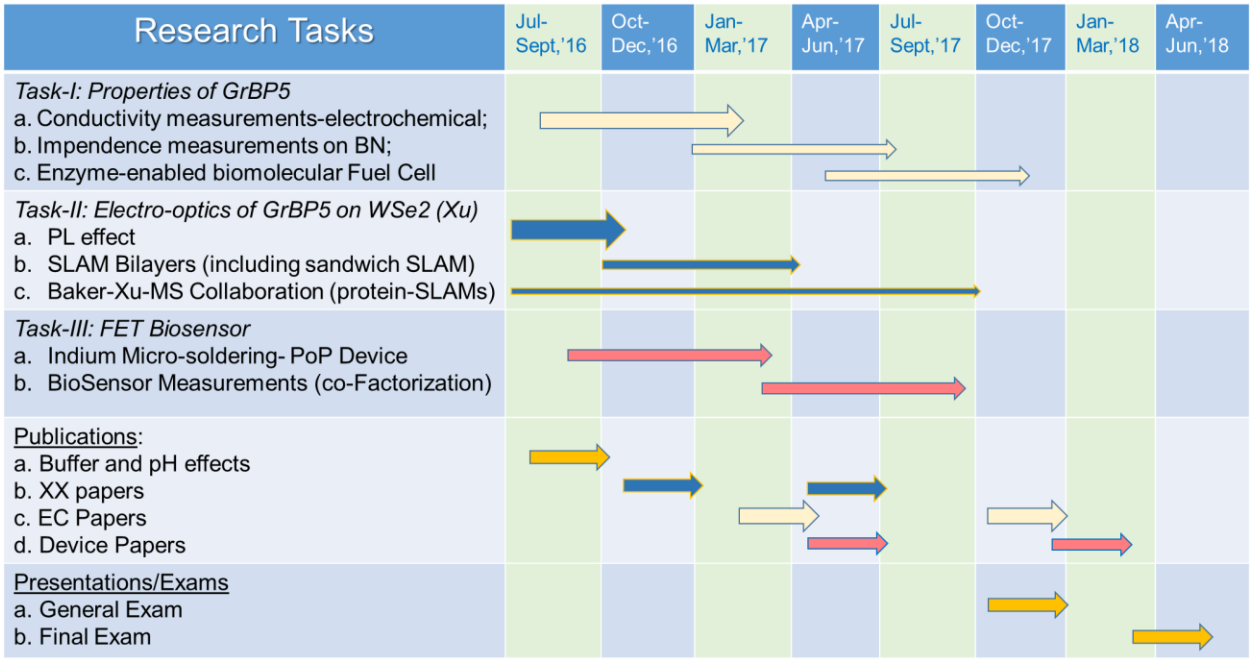

REFERENCES

[1] S.F. Oliveira, G. Bisker, N.A. Bakh, S.L. Gibbs, M.P. Landry, M.S. Strano. Protein functionalized carbon nanomaterials for biomedical applications, Carbon 95 (2015) 767-779.

[2] D. Khatayevich, M. Gungormus, H. Yazici, C. So, S. Cetinel, H. Ma, A. Jen, C. Tamerler, M. Sarikaya. Biofunctionalization of materials for implants using engineered peptides, Acta Biomaterialia 6 (2010) 4634-4641.

[3] L. Zhou, Y.Z. Lai, W.X. Huang, S.J. Huang, Z.Q. Xu, J. Chen, D. Wu. Biofunctionalization of microgroove titanium surfaces with an antimicrobial peptide to enhance their bactericidal activity and cytocompatibility, Colloids and Surfaces B-Biointerfaces 128 (2015) 552-560.

[4] D. Khatayevich, T. Page, C. Gresswell, Y. Hayamizu, W. Grady, M. Sarikaya. Selective Detection of Target Proteins by Peptide-Enabled Graphene Biosensor, Small 10 (2014) 1505-1513.

[5] G.K. Toworfe, R.J. Composto, I.M. Shapiro, P. Ducheyne. Nucleation and growth of calcium phosphate on amine-, carboxyl- and hydroxyl-silane self-assembled monolayers, Biomaterials 27 (2006) 631-642.

[6] M.D. Porter, T.B. Bright, D.L. Allara, C.E.D. Chidsey. Spontaneously Organized Molecular Assemblies .4. Structural Characterization of Normal-Alkyl Thiol Monolayers on Gold by Optical Ellipsometry, Infrared-Spectroscopy, and Electrochemistry., Journal of the American Chemical Society 109 (1987) 3559-3568.

[7] M. Schaeferling, S. Schiller, H. Paul, M. Kruschina, P. Pavlickova, M. Meerkamp, C. Giammasi, D. Kambhampati. Application of self-assembly techniques in the design of biocompatible protein microarray surfaces, Electrophoresis 23 (2002) 3097-3105.
[8] C.R. So, C. Tamerler, M. Sarikaya. Adsorption, Diffusion, and Self-Assembly of an Engineered Gold-Binding Peptide on Au(111) Investigated by Atomic Force Microscopy, Angewandte Chemie-International Edition 48 (2009) 5174-5177.
[9] X. Yu, Q.M. Wang, Y.A. Lin, J. Zhao, C. Zhao, J. Zheng. Structure, Orientation, and Surface Interaction of Alzheimer Amyloid-beta Peptides on the Graphite, Langmuir 28 (2012) 6595-6605.
[10] B.L. Coyle, M. Rolandi, F. Baneyx. Carbon-Binding Designer Proteins that Discriminate between sp(2)- and sp(3)-Hybridized Carbon Surfaces, Langmuir 29 (2013) 4839-4846.
[11] X.B. Mao, Y.Y. Guo, Y. Luo, L. Niu, L. Liu, X.J. Ma, H.B. Wang, Y.L. Yang, G.H. Wei, C. Wang. Sequence Effects on Peptide Assembly Characteristics Observed by Using Scanning Tunneling Microscopy, Journal of the American Chemical Society 135 (2013) 2181-2187.
[12] Y. Baskin, L. Meyer. LATTICE CONSTANTS OF GRAPHITE AT LOW TEMPERATURES, Physical Review 100 (1955) 544-544.
[13] A.H. Castro Neto, F. Guinea, N.M.R. Peres, K.S. Novoselov, A.K. Geim. The electronic properties of graphene, Reviews of Modern Physics 81 (2009) 109-162.
[14] D.O. Perevezentseva, E.V. Gorchakov. Voltammetric determination of cysteine at a graphite electrode modified with gold nanoparticles, Journal of Solid State Electrochemistry 16 (2012) 2405-2410.
[15] M.H. Cho, J. Ju, S.J. Kim, H. Jang. Tribological properties of solid lubricants (graphite, Sb2S3, MoS2) for automotive brake friction materials, Wear 260 (2006) 855-860.
[16] J. Aagaard. The Carbomedics aortic heart valve prosthesis: A review, Journal of Cardiovascular Surgery 45 (2004) 531-534.
[17] K.S. Novoselov, A.K. Geim, S.V. Morozov, D. Jiang, Y. Zhang, S.V. Dubonos, I.V. Grigorieva, A.A. Firsov. Electric field effect in atomically thin carbon films, Science 306 (2004) 666-669.
[18] A. Castellanos-Gomez, R.H.M. Smit, N. Agrait, G. Rubio-Bollinger. Spatially resolved electronic inhomogeneities of graphene due to subsurface charges, Carbon 50 (2012) 932-938.
[19] C.S. Shan, H.F. Yang, J.F. Song, D.X. Han, A. Ivaska, L. Niu. Direct Electrochemistry of Glucose Oxidase and Biosensing for Glucose Based on Graphene, Analytical Chemistry 81 (2009) 2378-2382.
[20] H.T. Liu, Y.Q. Liu, D.B. Zhu. Chemical doping of graphene, Journal of Materials Chemistry 21 (2011) 3335-3345.
[21] C.R. So, Y. Hayamizu, H. Yazici, C. Gresswell, D. Khatayevich, C. Tamerler, M. Sarikaya. Controlling Self-Assembly of Engineered Peptides on Graphite by Rational Mutation, Acs Nano 6 (2012) 1648-1656.
[22] J.C. Berg. An introduction to interfaces & colloids : the bridge to nanoscience, World Scientific, Singapore; Hackensack, NJ, 2010.
[23] S.M. Notley. Highly Concentrated Aqueous Suspensions of Graphene through Ultrasonic Exfoliation with Continuous Surfactant Addition, Langmuir 28 (2012) 14110-14113.
[24] V.K. Paruchuri, A.V. Nguyen, J.D. Miller. Zeta-potentials of self-assembled surface micelles of ionic surfactants adsorbed at hydrophobic graphite surfaces, Colloids and Surfaces a-Physicochemical and Engineering Aspects 250 (2004) 519-526.

[25] B. Rezacova, Y.M. Coic, C. Zentz, P.Y. Turpin, J. Stepanek. Spectroscopic Determination of pKa Constants of MADS Box Segments, Spectroscopy-an International Journal 27 (2012) 455-461.
[26] M. Sela, E. Katchalski. SPECTROPHOTOMETRIC TITRATION OF ALPHA-AMINO ACID COPOLYMERS CONTAINING TYROSINE, Journal of the American Chemical Society 78 (1956) 3986-3989.
[27] J.N. Israelachvili. Intermolecular and surface forces : with applications to colloidal and biological systems, Academic Press, London ; Orlando, Fla . 1985.
[28] K. Chen, Z.L. Zhang, Y.M. Liang, W. Liu. A Graphene-Based Electrochemical Sensor for Rapid Determination of Phenols in Water, Sensors 13 (2013) 6204-6216.
[29] T.R. Page, Y. Hayamizu, C.R. So, M. Sarikaya. Electrical detection of biomolecular adsorption on sprayed graphene sheets, Biosensors & Bioelectronics 33 (2012) 304-308.
[30] M. Garvey, K. Tepper, C. Haupt, U. Knupfer, K. Klement, J. Meinhardt, U. Horn, J. Balbach, M. Fandrich. Phosphate and HEPES buffers potently affect the fibrillation and oligomerization mechanism of Alzheimer's A beta peptide, Biochemical and Biophysical Research Communications 409 (2011) 385-388.
[31] M. Levitt, M. Hirshberg, R. Sharon, V. Daggett. POTENTIAL-ENERGY FUNCTION AND PARAMETERS FOR SIMULATIONS OF THE MOLECULAR-DYNAMICS OF PROTEINS AND NUCLEIC-ACIDS IN SOLUTION, Computer Physics Communications 91 (1995) 215-231.
[32] M. Levitt, M. Hirshberg, R. Sharon, K.E. Laidig, V. Daggett. Calibration and testing of a water model for simulation of the molecular dynamics of proteins and nucleic acids in solution, Journal of Physical Chemistry B 101 (1997) 5051-5061.
[33] D. Khatayevich, C.R. So, Y. Hayamizu, C. Gresswell, M. Sarikaya. Controlling the Surface Chemistry of Graphite by Engineered Self-Assembled Peptides, Langmuir 28 (2012) 8589-8593.
[34] X.S. Li, W.W. Cai, J.H. An, S. Kim, J. Nah, D.X. Yang, R. Piner, A. Velamakanni, I. Jung, E. Tutuc, S.K. Banerjee, L. Colombo, R.S. Ruoff. Large-Area Synthesis of High-Quality and Uniform Graphene Films on Copper Foils, Science 324 (2009) 1312-1314.
[35] X.S. Li, C.W. Magnuson, A. Venugopal, R.M. Tromp, J.B. Hannon, E.M. Vogel, L. Colombo, R.S. Ruoff. Large-Area Graphene Single Crystals Grown by Low-Pressure Chemical Vapor Deposition of Methane on Copper, Journal of the American Chemical Society 133 (2011) 2816-2819.
[36] J. Cho, L. Gao, J.F. Tian, H.L. Cao, W. Wu, Q.K. Yu, E.N. Yitamben, B. Fisher, J.R. Guest, Y.P. Chen, N.P. Guisinger. Atomic-Scale Investigation of Graphene Grown on Cu Foil and the Effects of Thermal Annealing, Acs Nano 5 (2011) 3607-3613.
[37] H.I. Rasool, E.B. Song, M.J. Allen, J.K. Wassei, R.B. Kaner, K.L. Wang, B.H. Weiller, J.K. Gimzewski. Continuity of Graphene on Polycrystalline Copper, Nano Letters 11 (2011) 251-256.
[38] J.A. Wilson, A.D. Yoffe. TRANSITION METAL DICHALCOGENIDES DISCUSSION AND INTERPRETATION OF OBSERVED OPTICAL, ELECTRICAL AND STRUCTURAL PROPERTIES, Advances in Physics 18 (1969) 193-&.
[39] V. Podzorov, M.E. Gershenson, C. Kloc, R. Zeis, E. Bucher. High-mobility field-effect transistors based on transition metal dichalcogenides, Applied Physics Letters 84 (2004) 3301-3303.

[40] A. Ayari, E. Cobas, O. Ogundadegbe, M.S. Fuhrer. Realization and electrical characterization of ultrathin crystals of layered transition-metal dichalcogenides, Journal of Applied Physics 101 (2007) 5.
[41] K.F. Mak, C. Lee, J. Hone, J. Shan, T.F. Heinz. Atomically Thin MoS2: A New Direct-Gap Semiconductor, Physical Review Letters 105 (2010) 4.
[42] B. Radisavljevic, M.B. Whitwick, A. Kis. Integrated Circuits and Logic Operations Based on Single-Layer MoS2, Acs Nano 5 (2011) 9934-9938.
[43] Q.H. Wang, K. Kalantar-Zadeh, A. Kis, J.N. Coleman, M.S. Strano. Electronics and optoelectronics of two-dimensional transition metal dichalcogenides, Nature Nanotechnology 7 (2012) 699-712.
[44] Q.Y. He, Z.Y. Zeng, Z.Y. Yin, H. Li, S.X. Wu, X. Huang, H. Zhang. Fabrication of Flexible MoS2 Thin-Film Transistor Arrays for Practical Gas-Sensing Applications, Small 8 (2012) 2994-2999.
[45] N. Alem, R. Erni, C. Kisielowski, M.D. Rossell, W. Gannett, A. Zettl. Atomically thin hexagonal boron nitride probed by ultrahigh-resolution transmission electron microscopy, Physical Review B 80 (2009) 7.
[46] C.R. Dean, A.F. Young, I. Meric, C. Lee, L. Wang, S. Sorgenfrei, K. Watanabe, T. Taniguchi, P. Kim, K.L. Shepard, J. Hone. Boron nitride substrates for high-quality graphene electronics, Nature Nanotechnology 5 (2010) 722-726.
[47] M. Briman, N.P. Armitage, E. Helgren, G. Gruner. Dipole relaxation losses in DNA, Nano Letters 4 (2004) 733-736.
[48] C. Zhong, Y.X. Deng, A.F. Roudsari, A. Kapetanovic, M.P. Anantram, M. Rolandi. A polysaccharide bioprotonic field-effect transistor, Nature Communications 2 (2011) 5.
[49] C.O. Girit, A. Zettl. Soldering to a single atomic layer, Applied Physics Letters 91 (2007) 3.
[50] P. Rivera, J.R. Schaibley, A.M. Jones, J.S. Ross, S.F. Wu, G. Aivazian, P. Klement, K. Seyler, G. Clark, N.J. Ghimire, J.Q. Yan, D.G. Mandrus, W. Yao, X.D. Xu. Observation of long-lived interlayer excitons in monolayer MoSe2-WSe2 heterostructures, Nature Communications 6 (2015) 6.
[51] J.S. Ross, S.F. Wu, H.Y. Yu, N.J. Ghimire, A.M. Jones, G. Aivazian, J.Q. Yan, D.G. Mandrus, D. Xiao, W. Yao, X.D. Xu. Electrical control of neutral and charged excitons in a monolayer semiconductor, Nature Communications 4 (2013) 6.
[52] E. Lojou. Hydrogenases as catalysts for fuel cells: Strategies for efficient immobilization at electrode interfaces, Electrochimica Acta 56 (2011) 10385-10397.